Localized intercellular transfer of ephrin-As by trans-endocytosis enables long-term signaling

José Ignacio Valenzuela, Franck Perez

Localized intercellular transfer of ephrin-As by trans-endocytosis enables long-term signaling

José Ignacio Valenzuela[1]*, Franck Perez[1,2]*

Affiliations:

[1]Institut Curie, PSL Research University, CNRS, UMR144, 26 rue d'Ulm, F-75005, Paris, France.

[2] Lead contact

*Correspondence: jose-ignacio.valenzuela@curie.fr (J.I.V.), franck.perez@curie.fr (F.P.)

Summary

Ephrins can elicit either contact-mediated cell-cell adhesion or repulsion, depending on the efficiency of removal of their ligand/receptor complexes from the cell surface, thus controlling tissue morphogenesis and oncogenic development. However, the dynamic of turnover of the newly assembled ephrin/Eph complexes during cell-cell interactions remains mostly unexplored. Here we show that ephrin-A1/EphA2 complexes are locally formed at the tip of filopodia, at cell-to-cell contacts. Clusters of ephrin-A1 from donor cells surf on filopodia associated to EphA2-bearing sub-domains of acceptor cells. Full-length ephrin-A1 is transferred to acceptor cells by trans-endocytosis through a proteolysis-independent mechanism. Trans-endocytosed ephrin-A1 bound to its receptor enables signaling to be emitted from endo-lysosomes of acceptor cells. Localized trans-endocytosis of ephrin-A1 sustains contact-mediated repulsion on cancer cells. Our results uncover the essential role played by local concentration at the tip of filopodia and the trans-endocytosis of full-length ephrin to maintain long-lasting ephrin signaling.

Introduction

Cell contact-mediated repulsion is a basic mechanism of cell and axon navigation that underlies tissue boundary formation and patterning (Batlle and Wilkinson, 2012). The fundamental principle relies on the high-affinity interaction between a surface-bound repellent and its receptor on opposing cell. The repellent-receptor complexes form a physical tether that must be removed after cell-cell contact to allow cell detachment and repulsion. This can be achieved by two conceptually different mechanisms: i) regulated cleavage of the ligand-receptor complex (Hattori et al., 2000; Janes et al., 2005), ii) trans-endocytosis of the complete ligand-receptor cluster (Gaitanos et al., 2016; Marston et al., 2003; Zimmer et al., 2003). Eph receptors (EphRs) are the largest subfamily of tyrosine kinases receptors and together with ephrins, their membrane-bound ligands, constitute important cell guiding cues during development and oncogenesis (Batlle and Wilkinson, 2012; Boyd et al., 2014; Kania and Klein, 2016). EphRs activate signaling pathways that directly impact cytoskeleton regulating cell-cell interactions, guiding cell migration, neuronal pathfinding and tissue patterning (Kania and Klein, 2016). EphRs are classified into two subfamilies; EphA and EphB, depending on the membrane anchoring nature of the ligand they preferentially bind, either glycophosphatidylinositol (GPI)-anchored ephrins (ephrin-As type) or transmembrane ephrins (ephrin-Bs type) respectively (Eph Nomenclature Committee, 1997). Ephrin's linkage to membranes facilitates its clustering, which is essential for the efficient receptor activation (Davis et al., 1994; Stein et al., 1998). The membrane localization of the ligands provides to the ephrin-Eph pathway the unique property of transducing reverse signals into the cells that express the ligand, in addition to the forward signals in the cells that contain the EphRs (Klein, 2009; Pasquale, 2008).

Under the current paradigm of ephrin-mediated repulsion, ephrin-B/EphB cell tethers are removed from the cell surface by trans-endocytosis of the whole complex including portions of the surrounding membranes (Marston et al., 2003), by a mechanism that is bidirectional (Gaitanos et al., 2016; Zimmer et al., 2003) and depends on the intracellular domains of both proteins and the Rac pathway (Gaitanos et al., 2016; Marston et al., 2003;

Zimmer et al., 2003). In contrast, ephrin-A/EphA cell tethers are broken by the controlled proteolysis of the ephrin ectodomain followed by endocytosis of the cleaved ligand-receptor complex (Greene et al., 2014; Hattori et al., 2000; Janes et al., 2005, 2009; Yoo et al., 2011). The main metalloprotease involved in the ephrin-A cleavage is ADAM10 (A disintegrin and metalloprotease 10). Thereby, ephrin-A2 and ephrin-A5 are cleaved by ADAM10 which may act both in *cis* or *trans* (Hattori et al., 2000, Janes et al., 2005, 2009). ADAM10 is recruited to sites of ephrin-A1/EphA2 interaction where ephrin-A1 removal from membranes is sensitive to ADAM10/17 inhibition (Greene et al., 2014). Ephrin-A1 might also be processed by ADAM12 (Ieguchi et al., 2014). While proteolytic cleavage of ephrin-B/EphB have also been observed (Georgakopoulos et al., 2006; Litterst et al., 2007; Tomita et al., 2006), only the shedding mechanism has been reported for the ephrin-A/EphA-dependent cell-to-cell detachment.

The spatial organization of the EphRs at the plasma membrane (PM) is essential for their response to ephrins and subsequent endocytosis (Davis et al., 1994; Greene et al., 2014; Schaupp et al., 2014; Seiradake et al., 2013; Shaw et al., 2014; Stein et al., 1998). Nevertheless, very little is known about the arrival to the PM of ephrins and EphRs and how it defines the sites of assembly and removal of the cell tether during cell-cell interactions. Here, we have synchronized the secretory trafficking of ephrin-As and its receptor in order to control their membrane delivery and spatiotemporally characterize the subcellular dynamics and fate of their signaling complexes under a native membrane context. We focused on the trafficking of ephrin-A1 and its receptor EphA2. EphA2 is frequently overexpressed and associated with poor prognosis in many different types of cancer (Boyd et al., 2014; White and Getsios, 2014; Wykosky and Debinski, 2008). Here we report that ephrin-A1 locally forms signaling clusters with EphA2Rs on opposing cells at sites of filopodia-filopodia and filopodia-cell interaction. Receptor-expressing cells internalize full-length ephrin-A1. Importantly, we show that trans-endocytosis of ephrin-A1 is independent of its cleavage. This adds a new layer of complexity to the accepted model of how ephin-As regulate cell-to-cell contact and reveals the unexpected

role of the trans-endocytosis of ephrin to sustain long-lasting signaling from endomembranes.

Results

Synchronization of the secretion of EphA2 and ephrin-A1

To finely tune the delivery of EphA and ephrin-As to the PM we used the RUSH (Retention Using Selective Hooks) system (Boncompain et al., 2012). RUSH allows the synchronization of the secretory trafficking of a chosen protein using biotin-sensitive cargo retention in the ER (Fig. 1A). We focused on the trafficking of ephrin-A1 and its receptor EphA2. We used HeLa cells because their morphology allows to easily identify various cellular compartment and they recapitulate *in vitro* the cell signaling through filopodia that have been observed *in vivo* (Lidke et al., 2005; Moti et al., 2019). We performed simultaneous live-cell imaging of SBP-Cherry-ephrin-A1 and EphA2-EGFP-SBP. Both cargoes were efficiently retained in the ER and rapidly exported from it after biotin addition, reaching the Golgi apparatus (GA) in ~5 min (Fig. 1 C, D). We measured the fluorescence intensity of the cargoes at the GA over the time as an indication of their trafficking kinetic. We observed that both cargoes peak at ~15 min (Fig. 1C, D) before experiencing an intra-GA segregation. A difference in GA exit kinetic is also observed, with ephrin-A1 residing longer than EphA2 in the GA (Fig. 1C to E and video S1). This coincides with the sorting of EphA2 and ephrin-A1, which are partially segregated in post-Golgi vesicles in route to the PM (Fig. 1C, E). As expected, and as a control, SBP-EGFP-ephrin-A1 and SBP-Cherry-ephrin-A1 fully co-localized during their secretory transport (Fig. 1E and video S1).

We observed that ephrin-A1, but not EphA2 was concentrated in filopodia-associated subdomains of the PM upon arriving at the cell surface (Fig. 1F). It then seemed to be exported into neighboring cells at later time points. We imaged the trafficking of SBP-EGFP-ephrin-A1 in live-cells co-expressing a mCherry-tagged PM marker (PM-Cherry). We observed that ephrin-A1 clusters were formed at the base or all along filopodia ~20 min

after biotin addition, where they often localize at the tip before being exported from ligand producing cells later on (Fig. 1G-I and video S2).

Eprhin-As are sorted into signaling filopodia

This phenomenon was also observed for another GPI-anchored ephrin-A. ephrin-A5 (SBP-EGFP-ephrin-A5) was also targeted to, and released from, the tip of filopodia upon arriving at the cell surface (Fig. 2A, and video S3). This suggests that the localized secretion on filopodia may be a general behavior for ephrin-As. We tested if this was a common behavior of GPI-anchored proteins (GPI-APs). We used the RUSH system to co-express ephrin-A1 together with different GPI-APs: a fully synthetic one (SBP-Cherry-GPI) or the naturally occurring GPI-APs (SBP-Cherry-CD59 and SBP-Cherry-ALPP). While all the GPI-APs we analyzed were co-transported with ephrin-A1 at early stages, they were excluded from the ephrin-A1-specific clusters at the PM and were not exported from transfected cells (Fig. 2B and video S4).

Because ephrin-A1 clusters were secreted from actin-rich filopodia, as visualized with the actin-binding peptide F-tractin-EGFP (Belin et al., 2014) (Fig. 2C), we questioned the role of actin dynamics in this process. We used cytochalasin-D to depolymerize actin in cells co-transfected with SBP-EGFP-ephrin-A1 and PM-Cherry. Live-cell imaging in control cells confirmed that, as observed above for SBP-EGFP- ephrin-A5, SBP-EGFP-ephrin-A1 clusters were only formed at the cell-cell interfaces (Fig. 2A and D, video S3 and S5). Interestingly, single filopodia can support many rounds of ephrin-A1 export, with the clusters being subsequently detected into neighboring cells. Surprisingly, despite the decrease in number and length of filopodia observed after actin disorganization (Fig. 2F-G), ephrin-A1 clusters were still produced with timing comparable to control cells. However they were rarely found at the tips of cellular extension and their transfer to neighboring cells was strongly impaired (Fig. 2D-E and H, video S5). End-point quantifications of fixed cells showed a significant decrease in the number of transferred ephrin-A1 clusters to the surrounding cells after cytochalasin-D or latrunculin-A treatments

(Fig. 2H). These data suggest that newly synthetized ephrin-As might be targeted to specialized signaling filopodia and that transport to surrounding cells is actin-dependent.

Cleavage-independent trans-endocytosis of ephrin-A1

Our experiments suggested that ephrin-A1 was transferred from ligand-producing cells (donor) towards acceptor cells, but it was still possible that these externalized clusters existed outside from neighboring cells. We thus evaluated whether externalized ephrin-A1 clusters were localized inside acceptor cells. We induced the delivery of SBP-EGFP-ephrin-A1 to the PM using the RUSH system, stopped the transport on ice and immunolabeled extracellular SBP-EGFP-ephrin-A1 in non-permeabilizing conditions. Then we permeabilized the cells and stained the total SBP-EGFP-ephrin-A1. Clusters immunostained only after permeabilization thus corresponded to an intracellular pool of ephrin-A1. Such clusters were clearly detected inside acceptor cells, implicating that ephrin-A1 expressed on a donor filopodia underwent endocytosis into acceptor cells (Fig. 3A).

To explain how a membrane-attached ephrin-A1 could be transferred to neighboring cells we examined whether it was cleaved at the tip of filopodia by ADAMs. We synchronized the trafficking of SBP-Cherry-ephrin-A1 after inhibition of ADAMs with the broad spectrum inhibitor TAPI-1 (Janes et al., 2005). Surprisingly, the intercellular transfer of ephrin-A1 from filopodia remained unaffected under ADAM inhibition (Fig. 3B, C), suggesting that it can proceed independently of proteolytic shedding, in contrast to proposed models (Greene et al., 2014; Hattori et al., 2000; Janes et al., 2005, 2009). It was however still possible that inhibition was incomplete or that an unrelated protease was responsible for the cleavage. Thus, we developed a fluorescent assay to unambiguously determine whether full-length ephrin-As can undergo trogocytosis as reported for ephrin-Bs (Gaitanos et al., 2016; Gong et al., 2019; Marston et al., 2003; Zimmer et al., 2003). We engineered a fusion protein, which consists of ephrin-A1 tagged at its N-terminal extremity with SBP-mCherry and at its C-terminal end, just before the GPI-anchor sequence, by EGFP (SBP-Cherry-ephrin-A1-EGFP-GPI) (Fig. 3D-F). Depending on the mode of

transfer of ephrin-A1, two possible output were expected: i) if ephrin-A1 was transferred to the acceptor cells as a product of its proteolytic cleavage, the clusters in the acceptor cells should be mCherry-positive and EGFP-negative, conversely ii) if ephrin-As were transferred without being cleaved, the clusters in the acceptor cells should be both mCherry-positive and EGFP-positive. Imaging synchronized transport of SBP-Cherry-ephrin-A1-EGFP-GPI to the cell surface, we consistently observed that clusters of ephrin-A1 positive for both mCherry and EGFP were trans-endocytosed from donor filopodia by the acceptor cells (Fig. 3D-F and video S6A). As a control, we inserted two consensus ADAM cleavage sites (2xADAMtide) (Caescu et al., 2009) between SBP-mCherry and the N-terminal of ephrin-A1-EGFP-GPI (SBP-Cherry-2xADAMtide-ephrin-A1-EGFP-GPI) (Fig. S1A). When SBP-Cherry-2xADAMtide-ephrin-A1-EGFP-GPI arrived to the PM, ADAMs induced the shedding of the SBP-Cherry portion and green, but not red, clusters were transferred to the acceptor cells (Fig. S1B-D). Importantly, the cleavage of SBP-Cherry-2xADAMtide-ephrin-A1-EGFP-GPI was efficiently reverted after ADAM inhibition with TAPI-1 or GI254023X (Fig. S1E-J).

Our data indicated that ephrin-A1 is trans-endocytosed in cleavage-independent manner. Two possible mechanisms were considered: the trans-endocytosis of ephrin-A1 may depend on the removal of the GPI-anchors (i.e. by phospholipase C), or full-length ephrin-A1 may be trans-endocytosed as a GPI-AP. To distinguish between these possibilities we designed a chimera in which we replaced the GPI-anchor sequence of SBP-Cherry-ephrin-A1 by the transmembrane domain of ephrin-B1 (EB1) followed by an EGFP in the cytoplasmic domain (SBP-Cherry-ephrin-A1-TMD-EB1-EGFP). If trans-endocytosis of ephrin-A1 depends on GPI-anchor cleavage, the ephrin chimera should stay bound to the PM of the donor cell and should not be transferred to the acceptor cells. On the contrary, if the whole ephrin-A undergoes trans-endocytosis, transfer may occur and the trans-endocytosed clusters should be mCherry- and EGFP-positive. Live-cell imaging revealed that clusters of SBP-Cherry-ephrin-A1-TMD-EB1-EGFP were pinched-off from the donor filopodia and trans-endocytosed as mCherry- and EGFP-positive clusters (Fig. 2G-I and

video S6B). Our results thus demonstrate that ephrin-As can be transferred to neighboring cells as full-length proteins probably by trogocytosis.

Dynamin-dependent trans-endocytosis of ephrin-A1 from cytonemes

There are two main structures reported to connect donor and target cells through filopodia-based membrane bridges, namely cytonemes and tunneling nanotubes (TNTs) (Sherer and Mothes, 2008). Cytonemes are specialized filopodia that connect distant cells through synaptic-like contacts, transporting signaling molecules, participating, for example, to establish a gradient of membrane bound morphogens *in vivo* (Kornberg and Roy, 2014). Unlike cytonemes, TNTs are cell extensions that directly connect the cytoplasm of donor and acceptor cells, enabling the intercellular transfer of cytosolic content such as protein aggregates, endosomes and lysosomes (Abounit et al., 2016; Burtey et al., 2015; Gousset et al., 2009; Sherer and Mothes, 2008). In contrast to cytonemes, intercellular transfer of cargoes through TNTs is insensitive to endocytosis block (e.g. dynamin inhibition) (Abounit et al., 2016; Burtey et al., 2015). Thus, to differentiate between both mechanisms, we first inhibited dynamin-dependent endocytosis by pre-incubating SBP-EGFP-ephrin-A1 transfected cells and acceptor cells with the dynamin inhibitor Dyngo4A. Dyngo4A treatment efficiently inhibited endocytosis (as seen by transferrin uptake) as well as the intercellular transfer of SBP-EGFP-ephrin-A1 (Fig. 4A-C). We further blocked dynamin-dependent endocytosis specifically in acceptor cells by co-culturing SBP-EGFP-ephrin-A1 expressing cells with cells overexpressing either wild-type dynamin-1-CFP (Dynamin-1-WT) or the GTPase-defective/dominant-negative dynamin-1 (Dynamin-1-K44A). As expected, ephrin-A1 clusters were efficiently transferred through SBP-EGFP-ephrin-A1/Dynamin-1-WT interfaces (Fig. 4D and video S7). However, the internalization of ephrin-A1 clusters was strongly inhibited in Dynamin-1-K44A expressing cells, tending to accumulate at the donor/acceptor interface (Fig. 4D and video S7). These data indicate that ephrin-A1 is trans-endocytosed from cytoneme-like filopodia rather than transferred through TNTs.

We then analyzed the endocytic pathway followed by ephrin-A1 upon transfer into receiving cells. SBP-EGFP-ephrin-A1 expressing cells were mixed with cells expressing either wild-type or GTP-locked Rab5 mutant (mRFP-Rab5-WT or mCherry-Rab5-Q79L, respectively). Rab5 localizes at early endosomes and its GTP-bound form causes early endosome fusion. Importantly, mCherry-Rab5-Q79L expression in acceptor cells blocked ephrin-A1 inside Rab5-enlarged endosomes (Fig. 4E). Early endosomes-bearing trans-endocytosed ephrin-A1 mature to late endosomes, as visualized by the co-culture of SBP-Cherry-ephrin-A1 expressing cells with cells expressing Rab7 (EGFP-Rab7-WT) or the active GTPase-deficient mutant of Rab7 (EGFP-Rab7-Q76L) (Fig 4F). In contrast, trans-endocytosed ephrin-A1 is sorted apart from recycling endosomes, as indicated by the same type of experiments done using cells overexpressing Rab11 (EGFP-Rab11-WT) or the dominant negative GDP-bound form of Rab11 (DsRed-Rab11-S25N) (Fig. S2).

Localized trans-endocytosis of ephrin-A1 in complex with EphA2

We wondered whether the high local concentration of ephrin-A1 at filopodia tip might confine the ephrin signaling. We performed immunostaining after SBP-EGFP-ephrin-A1 secretion using an anti-phosphotyrosine antibody or an antibody that recognizes the active form of the EphARs (pEphA). We observed a strong co-localization between ephrin-A1 clusters and either phosphotyrosine signal or pEphA at the PM and inside the acceptor cells (Fig. 5A). Signaling started at the PM because when trans-endocytosis was blocked, activation of EphARs was still observed (Fig S3A). Signaling at the cell surface was actually linked to trans-endocytosis. Pharmacological inhibition of EphA2 signaling with Dasatinib (Chang et al., 2008) efficiently impaired trans-endocytosis of ephrin-A1 (Fig. 5B and Fig. S3B). In these conditions, steady clusters of ephrin-A1 were observed at the interface between donor filopodia and acceptor cells (Fig. 5B-C).

To evaluate the dynamics of ephrin-A1/EphA2 signaling complexes, we co-cultured SBP-EGFP-ephrin-A1 expressing cells with EphA2-Cherry-SBP expressing cells and performed live-cell imaging upon trafficking synchronization. Under these conditions, EphA2-bearing cells extend filopodia towards the ephrin-A1-filopodia. We detected the local formation of

high-order ligand/receptor clusters in subdomains of trans-interaction between donor and acceptor filopodia (Fig. 5D). Ephrin-A1/EphA2 complexes were preferentially transported through EphA2-containing filopodia towards the cell body of the acceptor cells where they underwent trans-endocytosis (Fig. 5D and video S17) although we sometimes observed clusters of EphA2Rs being pulled towards the cell body of ephrin-A1-producing cells (Fig. 5D and video S8). We questioned the trans-endocytosis of EphA2 by synchronizing the trafficking of extracellular-tagged SBP-EGFP-EphA2 co-cultured with cells transfected with SBP-Cherry-ephrin-A1. (Fig. 5E-F). We observed that a minor population of EphA2Rs might also undergo intercellular transfer.

Long-lasting signaling of trans-endocytosed ephrin-A1/EphA2 complexes in cancer cells

RUSH-based synchronization of transport was essential to reveal filopodia-dependent trans-endocytosis, however the intercellular transfer of ephrin-A1 to EphA2-expressing cells was massive at steady state (no hook expression) (video S9). This ruled-out possible artifacts due to trafficking synchronization. We then monitored transfer in cells known to use the ephrin-A1/EphA2 feedback loop. We used the highly aggressive breast cancer cell MDA-MB231, because they connect to the endothelia through filopodia promoting the formation of a metastatic niche in mice (Connor et al., 2015). We co-cultured MDA-MB231 cells stably expressing SBP-EGFP-EphA2 (MDA-EphA2) with MDA-MB231 cells stably expressing SBP-Cherry-ephrin-A1 (MDA-ephrin-A1). Live imaging revealed that ephrin-A1 undergoes massive trans-endocytosis in a complex with the EphA2R. Intracellularly; ephrin-A1/EphA2 clusters accumulate into large and round endomembrane compartments of MDA-EphA2 cells (Fig. 6A). Ephrin-A1 was still detected inside those compartments more than 7 h after release from the ER. We analyzed whether MDA-MB231 cells use lysosomes for the long-term storage of ephrin-A1. We co-cultured donor SBP-Cherry-ephrin-A1 expressing cells with acceptor MDA-EphA2 cells and we labeled the lysosomes using the SiR-lysosome dye, which binds to the lysosomal proteinase cathepsin-D. We observed that ephrin-A1/EphA2 complexes are co-internalized and transported to large

endo-lysosomal compartments (Fig. S4). To analyze whether sustained signaling accompanied this internalization, we co-cultured donor MDA-ephrin-A1 cells with wild-type MDA-MB231 cells used as acceptors. We labeled the lysosomal-associated membrane protein 1 (LAMP1) and active pEphARs. This experiment showed that trans-endocytosed ephrin-A1 was stored in lysosomes as signaling complexes. To better characterize the signaling compartment, we assessed for the acidity and degradative properties of the ephrin-A1-lysosomes by live-cell imaging using the pH-sensitive dye lysotracker and the fluorogenic protease substrate DQ-BSA respectively. We observed that trans-endocytosed ephrin-A1 is trafficked to acidic lysosomes, but just a minor population was found in degradative lysosome (Fig. S4). Interestingly, ephrin-A1-positive endo-lysosomes were slightly larger and concentrated a significantly higher amount of active EphARs than their ephrin-A1-negative counterpart (Fig. 6B-D).

In addition to protease-dependent cleavage, trans-endocytosis may thus be an alternative mechanism to allow cell separation and repulsion upon ephrin signaling. To measure contact-mediated cell repulsion we used a cell-confrontation assay (Porazinski et al., 2016). It consists in a two-compartment cell culture insert separated by a fixed gap. After removal of the insert, cells migrate to fill the gap and opposing cells meet and establish cell-to-cell contacts. As a control, when two monolayers of MDA-ephrin-A1 cells were confronted, both populations stopped migrating upon contact (Fig. 7A, B), suggesting that no repulsion signal was emitted. In contrast, when acceptor MDA-EphA2 cells were confronted to donor MDA-ephrin-A1 cells, the acceptor MDA-EphA2 cells were repelled backward; meanwhile the MDA-ephrin-A1 cells persisted migrating forward (Fig. 7A, B). MDA-EphA2 repulsion correlated with the transfer of ephrin-A1 to acceptor cells, suggesting that trans-endocytosis of ephrin-A1 was used to remove the cell-cell tether formed by ephrin-A1 and EphA2.

Remarkably, when a MDA-EphA2 acceptor cell undergoes cell division short after ephrin-A1 trans-endocytosis, ephrin-A1 was inherited to the daughter cells inside an endomembrane compartment (Fig. 7C and video S10). To determine if activated EphARs

can be inherited during cell division, MDA-MB231 cells labeled with a cell dye were seeded on gridded cell dishes and synchronized at the G2 phase of the cell cycle with the CDK1 inhibitor RO3306. Then MDA-ephrin-A1 cells were seeded on top of the acceptor cells in presence of biotin. Once the acceptor endosomes were filled with ephrin-A1, biotin and RO3306 were washed out and we imaged live the acceptor cells mitosis (Fig. 7D). We corroborated that trans-endocytosed ephrin-A1 is transmitted to daughter cells. When acceptor cells completed mitosis, we fixed them and co-stained with antibodies against LAMP-1 and pEphA. Importantly, we observed that around 60% of the inherited ephrin-A1 was localized into lysosomes and about 40% of inherited ephrin-A1-clusters contained pEphA (Fig. 7D-E), suggesting that a memory of ephrin signaling might be transmitted over generations.

Discussion

Membrane-bound ephrins and EphRs are ubiquitous signaling molecules present in most of cell types and regulating a myriad of biological processes. The localization and clustering of ephrins at the PM is required for the efficient receptor activation (Davis et al., 1994; Stein et al., 1998), restricting the ephrin/Eph communication to the cell vicinity at sites of cell-to-cell contact. However, there are some exceptions to this juxtacrine ephrin signaling. Ephrin-A1 can be released in soluble forms by matrix metalloproteases activating an EphA2-dependent signaling at paracrine level (Beauchamp et al., 2012; Wykosky et al., 2008). Ectodomains of EphAs, EphBs and ephrin-Bs can also be released by proteolytic shedding, leading to signaling inhibition (Barquilla and Pasquale, 2015). Additionally, cells can display EphAs, EphBs and ephrin-Bs on extracellular vesicles (EVs); which would expand the signaling to the endocrine level (Gong et al., 2016). Ephrin-As and -Bs may thus differ on their mechanisms of long-range communication.

Here we have uncovered a mechanism supporting long-range action for ephrin-As, namely cytonemes. Contacts produced by cytonemes are considered as a subtype of synaptic signaling (Kornberg and Roy, 2014). Transport of ephrin-A on cytonemes brings several advantages: i) it allows ephrin-A to be concentrated at the tip of filopodia for efficient

signaling; ii) the length of these filopodia enables the cells to sustain long-distance communication with EphARs displayed on acceptor PM; iii) concentration of the ligand at the tip of a very fine structure allows its efficient trans-endocytosis. This phenomenon, while massive at steady state, may have been overlooked so far. Synchronization of transport allowed generating a pulse that revealed this phenomenon.

The RUSH system enables the coordinated delivery of ephrins and EphRs to the PM, which is a powerful approach to the study of ephrin signaling and trans-endocytosis without the need for artificial clustering of soluble and non-physiological ligands. PM association endows ephrins with the particularity of transduce bidirectional signaling (Pasquale, 2008). The fact that a small proportion of EphA2Rs are trans-endocytosed in ephrin-A1 producing cells suggests that bidirectional signaling may take place at cytonemes. Interestingly, in sea urchin embryos a transmembrane ephrin has been observed to localize to cytonemes at the basal surface of ectodermal cells (Krupke et al., 2016). In zebrafish, the ephrin-B1/EphB3b signaling regulates cytonemal contacts between hepatoblast and the adjacent lateral plate mesoderm, coordinating liver morphogenesis and laterality (Cayuso et al., 2016). In mammalian cells, myosin1b regulates the formation of filopodia at the ephrin-B1/EphB2 cellular interfaces, contributing to cell repulsion (Prospéri et al., 2015). Considering that ephrin-B/EphBR clusters are removed from the cell surface by trans-endocytosis (Gaitanos et al., 2016; Marston et al., 2003; Zimmer et al., 2003), it is reasonable to propose that filopodia localization and trans-endocytosis are closely linked signal transduction processes.

Importantly, we show that removal of ephrin-A/EphA complexes is cleavage-independent. This finding suggests an alternative to the accepted model of cell-tether removal and EphAR downregulation upon ephrin-A stimulation, which relies on the ADAM-dependent cleavage (Hattori et al., 2000; Janes et al., 2005, 2009). While it is still unclear whether trans-endocytosis has a distinct role from simple ephrin-A shedding, our results suggest that ADAMs might play an indirect role on cell-cell repulsion. For example, they may be used to regulate the shedding of E-cadherin, which have been observed on ephrin-B1/EphB

boundaries (Solanas et al., 2011) or the shedding of EGF and further down-regulation of E-cadherin, as shown for ephrin-A1/EphA2 cell interfaces (Kaplan et al., 2018). This would explain how the recruitment of ADAM10 to the ephrin-A/EphA interfaces can regulate repulsion independently of ephrin-A cleavage.

Ephrin-Bs also undergo bidirectional trogocytosis (Gaitanos et al., 2016; Gong et al., 2019; Marston et al., 2003; Zimmer et al., 2003), suggesting that all sorts of ephrins may be subjected to it. Trans-endocytosis of ephrin-As depends on actin. Similarly, actin and Rac1 have been reported to be involved in trans-endocytosis of ephrin-Bs (Gaitanos et al., 2016; Marston et al., 2003). Rac-1 has also been implicated in ephrin-A1-induced EphA2 endocytosis (Zhuang et al., 2007) and in ephrin-A5-induced EphA8 endocytosis during the development of the retinocollicuar topographic map in mice (Yoo et al., 2010, 2011). In neurons, ephrin-A2 induces Rac-1 activation, stimulating endocytosis in growth cones leading to their collapse (Jurney et al., 2002). We have shown that ephrin-As interact with EphARs at filopodia. In embryonic retinal explants, ephrin-A2 and EphA4 colocalize in axons regulating the density of axonal interstitial filopodia (Fiore et al., 2019). Early after birth, EphA4 receptors are located at the tip of axonal and dendritic filopodia in rat hippocampus (Tremblay et al., 2009). These data support the role of filopodia on ephrin-A-signaling *in vivo*.

Trogocytosed clusters of ephrin-A1 often contain small amounts of donor PM. In contrast to the shedding mechanism, trans-endocytosis allows the transfer of a membrane-attached ligand, hence keeping the ephrin in an oligomeric state and enabling efficient EphR activation. This would explain how trans-endocytosed ephrins are able to emit long-lasting signaling from lysosomes. Trans-endocytosed ephrin-A1/EphA2 complexes are transported using Rab5- and Rab7-endosomes (Fig. 7F). Similarly, fibroblast growth factor (FGF) forms a complex with cytoneme-localized FGF receptors and Rab5, which is retrogradely transported to the cell body (Koizumi et al., 2012). EGF (epidermal growth factor)/ErbB1 complexes are also endocytosed at the base of filopodia (Lidke et al., 2005), suggesting that different cytoneme-related signaling molecules may follow similar endocytic pathways.

Ephrin-A1-dependent EphA2 activation and internalization leads to a transient inactivation of ERK and Akt pathways (Sabet et al., 2015). Ephrin-A1-dependent Akt inhibition captures EGFR in Rab5 endosomes, therefore suppressing the pro-migratory Akt signaling from the PM while preserving proliferative endosomal ERK activity (Stallaert et al., 2018). In this context, cells with reduced cell-cell contact and therefore reduced ephrin signaling (e.g. at tissue boundaries) would increase their exploratory response to EGF, while cells located deeper into the tissue, would retain their proliferative response and fill the empty space despite their massive cell-cell contacts (Stallaert et al., 2018). A consequence of the endosomal sorting process is that it allows the transmission of ephrin-A/EphA complexes to the cellular progeny. This is possible because lysosomes are partitioned during cell division (Bergeland et al., 2001). Ephrin-loaded lysosomes may act then as long-term signaling unit, endowing the cell with a kind of memory. However, it will be essential to demonstrate that, in contrast to cleavage-dependent ephrin-A regulation, trans-endocytosis and complex storage in lysosomes provide a memory of signaling *in vivo*.

Long-distance communication through cytonemes, followed by storage in endomembranes may also promote the release of EphARs on EVs, switching to a cell contact-independent signaling modality (Fig. 7G). EphA2 on EVs may then both, activate reverse ephrin-signaling or titer down free ephrin-As on remote tissues. Because TNTs also participate in the intercellular transport of lysosomes (Abounit et al., 2016) they may help to transfer signaling lysosomes between cells. This might be especially important in tumor cells, in which specialized filopodia, were proposed to configure a network that provides resistance to therapies (Osswald et al., 2015). Notably, EphA2 overexpression decreases the sensitivity of breast cancer to tamoxifen and trastuzumab (Lu et al., 2003; Zhuang et al., 2010). It would be important to know if the potential transfer of lysosomes containing active EphA2Rs might spread a resistance to otherwise sensitive cells. A pending challenge is to decipher the role in both normal and pathological development of the pathway described here for ephrins, from transport and concentration on cytoneme to trans-endocytosis and long-term signaling. Such a pathway may also be at work for other signaling routes linking cell-cell adhesion to signaling and may represent a signature of cytoneme-based signaling.

Acknowledgments

The authors wish to thank V. Fraisier and L. Leconte from the PICT-IBiSA Lhomond Imaging facility of Institut Curie and the members of the Recombinant Antibodies Platform of the Institut Curie; Z. Gouveia for her help with lentiviral transductions; S. Divoux for her help with some experiments and G. Boncompain for constructs and advices; J. Ecard and M. Maurin for assistance with the Fiji macros. The work in the laboratory of F.P. was supported by the Institut Curie, the Centre National de la Recherche Scientifique (CNRS), the French Agence Nationale de la Recherche (ANR-12-BSV2-0003-01), Fondation Recherche Médicale (DEQ20120323723). LabEx CelTisPhyBio (ANR-10-LBX-0038 part of the IDEX PSL no. ANR-10-IDEX-0001-02; to FP and J.I.V.). Long-Term EMBO Fellowship (ALTF 607-2015) co-funded by the European Commission FP7 (Marie Curie Actions, LTFCOFUND2013, GA-2013-609409; to J.I.V.).

Author Contributions

J.I.V. conceived the study, conducted the experiments and analyzed the data. J.I.V. and F.P. designed the experiments and wrote the manuscript. F.P. supervised the study and acquired funding.

Declaration of Interests

The authors declare no competing interests.

Figure Legends

Figure 1 Synchronization of the secretion of EphA2 and ephrin-A1

(A) Scheme of the RUSH system.

(B) Scheme of SBP-Cherry-ephrin-A1 and EphA2-EGFP-SBP reporters.

(C) Time-lapse imaging of transport of SBP-Cherry-ephrin-A1 (red) and EphA2-EGFP-SBP (green) in a RUSH set-up (t = time after addition of biotin). Bottom panels (high-magnification images).

(D) Intensity plots of SBP-EGFP-ephrin-A1 or EphA2-EGFP-SBP at the GA (mean ± SEM).

(E) Percentage of colocalization (mean ± SEM) of EphA2-EGFP-SBP and SBP-Cherry-ephrin-A1 or SBP-EGFP-ephrin-A1 and SBP-Cherry-ephrin-A1. (D-E) Light red region is before Golgi exit, light green region is after Golgi exit.

(F) EphA2-EGFP-SBP (top panel, green) or SBP-EGFP-ephrin-A1 (bottom panel, green) transfected cells 90 min after biotin addition. Nuclei (magenta), GA (red). Right panels (high-magnification images). Arrows indicate filopodia.

(G) Live-cell imaging of the RUSH construct SBP-EGFP-ephrin-A1 (green) and the PM marker (PM-Cherry, red). Bottom panels (high-magnification images). Arrow indicates an ephrin-A1 cluster exported from filopodia.

(H) Temporal projection of SBP-EGFP-ephrin-A1 and PM-Cherry imaged live. Bottom panels (high-magnification images).

(I) Boxplot of the time of appearance of the first ephrin-cluster at the PM and the first ephrin-cluster exported from the PM.

(C, F-H) Scale bars, 10 μm. (*** $t<0.001$, two-tailed t-test) See also video S1 and S2.

Figure 2 ephin-As are sorted into signaling filopodia

(A) Live-cell imaging of the RUSH construct SBP-EGFP-ephrin-A5 (green) and the PM marker (PM-Cherry, red). F-actin (blue). Bottom panels (high-magnification images). (D) Donor cell, (A) Acceptor cell.

(B) Co-localization after synchronous transport to the cell surface of SBP-EGFP-ephrin-A1 with SBP-Cherry-GPI (left panels), SBP-Cherry-CD59 (middle panels) or SBP-Cherry-ALPP (right panels). ephrin-A1 (middle row), GPI reporters (bottom row). Nuclei (blue).

(C) Live-cell imaging of the RUSH construct SBP-Cherry-ephrin-A1 (red) and F-tractin-EGFP (green). Bottom panels (high-magnification images).

(D) Live-cell imaging of SBP-EGFP-ephrin-A1 (green) and PM-Cherry (red) under control conditions (top panels) or cytochalasin-D treatment (bottom panels). F-actin (blue).

(E) Kymographs analysis of one cluster of ephrin-A1 at cell-cell interface. The dotted line indicates the time of cluster formation.

(F) Number of filopodia in control (DMSO) and cytochalasin-treated (Cyto-D) cells (mean ± SD).

(G) Filopodia length distribution in control (DMSO) and cytochalasin-treated (Cyto-D) cells.

(H) Boxplot showing the normalized number of transferred ephrin-A1 clusters in control (DMSO) and cytochalasin-D (Cyto-D) or latranculin A-treated (Lat-A) cells. (A-D) Scale bars, 10 μm.

(F, H) * $t<0.05$; ** $t<0.01$; ** $t<0.01$, two tailed t-test. See also video S3-S5.

Figure 3 Cleavage-independent trans-endocytosis of ephrin-A1

(A) RUSH SBP-EGFP-ephrin-A1 (green) after 95 min of biotin addition. Surface ephrin-A1 (blue), total ephrin-A1 (red). Right panels (high-magnification images).

(B) RUSH SBP-Cherry-ephrin-A1 (red) in the presence (bottom) or absence (top) of TAPI-1. F-actin (green), nuclei (magenta). Right panels (high-magnification images).

(C) Boxplot of the normalized number of transferred ephrin-A1 clusters in control cells (DMSO) or cells treated with TAPI-1. (n.s., non-significant, two tailed t-test).

(D) Time-lapse imaging of the SBP-Cherry-ephrin-A1-EGFP-GPI sensor (drawn at the top). EGFP and Cherry signals are shown. Cell-cell boundaries are visualized with F-actin (blue). Bottom panels (high-magnification images).

(E) Kymograph analysis of one cluster of SBP-Cherry-ephrin-A1-EGFP-GPI into an acceptor cell.

(F) Line-scan analysis and EGFP/Cherry intensity ratio from (E).

(G-I) Same as in (D-F), but for the SBP-Cherry-ephrin-A1-TMD-ephrin-B1-EGFP sensor (drawn at the top). Red lines show a linear fit of the data.

(A-B, D-E, G-H) Scale bars, 10 μm. See also Fig. S1 and video S6.

Figure 4 Dynamin-dependent trans-endocytosis of ephrin-A1 from cytonemes

(A) Cells expressing SBP-EGFP-ephrin-A1 (green) and PM-Cherry (red) untreated (DMSO) or incubated with Dyngo4A and synchronized with biotin. Tfr-647 (cyan) shown endocytosed transferrin. Arrowheads indicate the clusters of ephrin-A1 inside acceptor cells.

(B) Line-scan analysis of colocalization between ephrin-A1 clusters and Tfr-647 endosomes.

(C) Boxplot of the normalized number of transferred ephrin-A1 clusters. (** $t<0.01$, two tailed t-test).

(D) SBP-EGFP-ephrin-A1-expressing cells (green) co-cultured with Dynamin-I-WT-CFP-expressing (blue, indicated with asterisks, top panels) or Dynamin-I-K44A-CFP-expressing cells (blue, indicated with asterisks, bottom panels). F-actin (red). Right panels (high-magnification images).

(E) Time-lapse imaging of SBP-EGFP-ephrin-A1-expressing cells (green) co-cultured with cells expressing mRFP-Rab5-WT (red, top panels) or Cherry-Rab5-Q79-L (red, bottom panels). Arrows indicate an example of trans-endocytosed SBP-EGFP-ephrin-A1 cluster in an acceptor cell. Arrowheads indicate an mRFP-Rab5-WT or Cherry-Rab5-Q79-L-positive endosomes. F-actin (blue).

(F) Same as (E) but for cells expressing SBP-Cherry-ephrin-A1 (red) co-cultured with cells expressing EGFP-Rab7-WT (green, top panels) or EGFP-Rab7-Q76-L (green, bottom panels).

(A, D-F) Scale bars, 10 μm. See also Fig. S2 and video S7.

Figure 5 Localized trans-endocytosis of ephrin-A1 in complex with EphA2

(A) SBP-EGFP-ephrin-A1 or SBP-Cherry-ephrin-A1 (green) expressing cells immuno-stained for phosphotyrosinated proteins (pTyrosine; top panels, red) or pEphARs (pEphA; bottom panels, red). Nuclei (blue). Right panels (high-magnification images).

(B) Time-lapse imaging of SBP-Cherry-ephrin-A1 (red) and PM-EGFP (green) under control conditions (upper panels) or after Dasatinib treatment. F-actin (blue). Arrows indicate stable clusters of ephrin-A1.

(C) Percentage of donor-acceptor interfaces in which we observed clustering and/or transfer or no clustering of ephrin-A1 (mean ± SEM).

(D) Mix culture of HeLa cells expressing SBP-EGFP-ephrin-A1 (green) or EphA2-Cherry-SBP (red) imaged live. F-actin (blue). The arrow indicates a failed phagocytosis of an EphA2-Cherry-SBP filopodia by a SBP-EGFP-ephrin-A1 expresing cell. High-magnifications images are presented below. SBP-EGFP-ephrin-A1 (top panels), EphA2-Cherry-SBP (bottom panels). Arrowheads indicate two events of filopodia-related co-internalization of SBP-EGFP-ephrin-A1 with EphA2-Cherry-SBP. Percentage of cell-cell interfaces in which EphA2-Cherry-SBP-cells behave as a donor, as an acceptor cell, or when the interfaces is bidirectional (mean ± SEM).

(E) RUSH SBP-Cherry-ephrin-A1 (red) cells co-cultured with SBP-EGFP-EphA2-expressing cells (green). Surface staining of SBP-EGFP-EphA2 (magenta). High-magnifications images (right panels). Arrowheads indicate clusters of SBP-EGFP-EphA2 trans-endocytosed into the ephrin-A1 expressing cells.

(F) Normalized number of transferred EphA2 clusters (mean ± SD).

(A-B, D-E) Scale bars, 10 μm. (C, F) * $t<0.05$; ** $t<0.01$, two tailed t-test. See also Fig. S3 and video S8-S9.

Figure 6 Long-lasting storage and signaling of trans-endocytosed ephrin-A1/EphA2 complexes in cancer cells

(A) Live-cell imaging of MDA-EGFP-EphA2 cells (green) co-cultured with MDA-Cherry-ephrin-A1 cells (red). High-magnification images: MDA-EGFP-EphA2 (top panels),

MDA-Cherry-ephrin-A1 (middle panels), merged images (bottom panels). Arrowheads indicate trans-endocytosed SBP-Cherry-ephrin-A1 stored inside the acceptor cell.

(B) HeLa cells expressing SBP-Cherry-ephrin-A1 (red) co-cultured with MDA-MB231-WT, co-stained with antibodies against LAMP1 (green) and pEphARs (white). Nuclei (blue). Right panels (high-magnification images) **(B')** High-magnification images of an individual lysosome boxed in B (right panels). Line-scan analysis (right plot) of ephrin-A1 (red), LAMP1 (green) and pEphA (gray).

(C) Plot showing the integrated intensity density (mean ± SD) of SBP-Cherry-ephrin-A1, LAMP1 and pEphA in acceptor MDA-MB-231-WT cells inside ephrin-A1-positive lysosomes (ephrin-A1+ / LAMP1+), ephrin-A1-negative lysosomes (ephrin-A1- / LAMP1+) or ephrin-A1- and lysosome-free cellular area (ephrin-A1- / LAMP1-).

(D) Lysosome area (μm^2) of ephrin-A1-positive and ephrin-A1-negative lysosomes (mean ± SD). (A-B) Scale bars, 10 μm; (B') scale bar 1 μm. (C-D) *t<0.05; ***t<0.001; n.s. non-significant, two tailed t-test. See also Fig. S4.

Figure 7 Trans-endocytosed ephrin-A1 participates in contact-mediated repulsion

(A) Cell confrontation assay of MDA-Cherry-ephrin-A1 labeled with a cell mask (left panels, green) confronted to MDA-Cherry-ephrin-A1 (left panels, red). Nuclei (blue). Trans-illumination images (gray). Right panels show a similar experiment done using MDA-EGFP-EphA2 (green) confronted to MDA-Cherry-ephrin-A1 cells (red). The cyan line depict the point of collision (time; h: min).

(B) Distance (μm) traveled by the marginal cells 20 h after collision (mean ± SD).

(C) Time-lapse of the collision and subsequent cell division of a MDA-Cherry-ephrin-A1 cell (red) with a MDA-EGFP-EphA2 cell (green). Trans-illumination images (gray). Capital letters indicates the donor cell (D), acceptor cell (A) and daughter cells (A', A'').

(D) Live-cell imaging of acceptor MDA-MB-231-WT cells labeled with a cell mask (A, green) co-cultured with donor MDA-Cherry-ephrin-A1 cells (D, red). Trans-illumination

images (gray). The timeline at the top summarizes the different steps of the experiment. Time indicates the time after washout of RO3306 (top panels). Correlative immunostaining with antibodies against pEphARs (blue) and LAMP1 (magenta, bottom panels). High-magnification of the boxed region (bottom right panels). Arrows indicate inherited ephrin-A1 clusters.

(E) Percentage of trans-endocytosed ephrin-A1 clusters co-localizing with LAMP-1, pEphA or both (mean ± SEM).

(F) Schematic model of the ephrin-As trans-endocytosis.

(G) Functional overview. Removal of the Ephrin-A/EphA cell tether by trans-endocytosis permits cell-cell repulsion to occur. Long-distance communication through cytonemes may promote the sorting of EphARs to multivesicular bodies (MVB) and/or to signaling lysosomes. EphARs can be secreted in extracellular vesicles (EVs) interacting with Ephrin-As on distant cells (green cell). Ephrin-A-containing lysosomes may also be transferred to neighboring cells through TNTs.

(A, C) Scale bars, 20 μm; (D) scale bars, 10 μm. (B, E) *t<0.05; ***t<0.001. two tailed t-test. See also video S10.

STAR Methods

LEAD CONTACT AND MATERIALS AVAILABILITY

Further information and request for reagents may be directed to, and will be fulfilled by the Lead Contact, Dr. Franck Perez (franck.perez@curie.fr). RUSH plasmids are already available through Addgene and we will deposit additional ones upon publication.

EXPERIMENTAL MODEL AND SUBJECT DETAILS

Cells and transfection

HeLa and MDA-MB231 wild-type cells were cultured in Dulbecco's modified Eagle medium (DMEM), high glucose, GlutaMAX™ (Life Technologies) supplemented with 10% fetal calf serum (FCS) (GE Healthcare), penicillin, streptomycin and 1mM sodium pyruvate (Life Technologies) at 37°C and 5% of CO_2. HeLa and MDA-MB231 stable cell lines expressing the streptavidin-KDEL hook (Boncompain et al., 2012) and the SBP-Cherry-ephrin-A1 or SBP-EGFP-EphA2 reporters (cloned in a pCDH-CMV-MCS-EF1α-Puro vector) were generated by transduction with lentiviral particles generated in HEK293T cells and cultured as described above, but supplemented with 4 μg/ml of puromycin (Invitrogen) and 0.5 mg/mL geneticin (Life Technologies). HeLa cells were transfected with calcium phosphate 24-48 h before fixation or imaging as previously described (Jordan et al., 1996).

METHOD DETAILS

Plasmids

RUSH plasmids of cargoes retain by their luminal domain (SBP-EGFP-ephrin-A1, SBP-Cherry-ephrin-A1, SBP-EGFP-ephrin-A5, SBP-EGFP-EphA2) were constructed as FseI/PacI inserts as previously described (Boncompain and Perez, 2012). SBP-Cherry-CD59 and SBP-Cherry-ALPP plasmids were previously published (Fourriere et al., 2019).

SBP-Cherry-GPI has been previously described (Boncompain et al., 2012) (Addgene plasmid #65295). Cytoplasmic retained EphA2 was amplified from pDONR223-EPHA2 (Johannessen et al., 2010) (Addgene plasmid #23926) and constructed like an AscI/MfeI insert (EphA2-EGFP-SBP and EphA2-Cherry-SBP) (Boncompain and Perez, 2012). SBP-Cherry-ephrin-A1-EGFP-GPI was generated by inserting the EGFP sequence (flanked by BamHI and XhoI sites) between the amino acids H181 and S182 of ephrin-A1. SBP-Cherry-ephrin-A1-TMD-ephrin-B1-EGFP contains the trans-membrane domain of ephrin-B1 (amino acids 229D to 279A) fuse to EGFP after the amino acid H181 of ephrin-A1. SBP-Cherry-2xADAMtide-ephrin-A1-EGFP-GPI was created by replacing the mCherry of the SBP-Cherry-ephrin-A1-EGFP-GPI construct by mCherry fused to 2 consensus ADAM cleavage sites (2XADAMtide: PRAEALKGGPRAEALKGG) (Caescu et al., 2009). The plasmid containing myristoylation and palmitoylation signals (MyrPalm) fused to EYFP (PM-EGFP) was kindly provided by Roger Y. Tsien (UCSD, USA) (Zacharias et al., 2002); PM-Cherry was generated by the insertion of the MyrPalm signals as a NheI/AgeI fragment in pmCherry-C1 (Takara Clontech). F-tractin-EGFP was a gift from Dyche Mullins (Belin et al., 2014) (Addgene plasmid #58473). Dynamin-1-WT-CFP and Dynamin-1-K44A-CFP were created by replacing the EGFP tag of Dynamin-1-WT-EGFP (Addgene plasmid #34680) or Dynamin-1-K44A-EGFP (Addgene plasmid #34681) by CFP (Song et al., 2004). mRFP-Rab5-WT was kindly provided by Marino Zerial (MPI-CBG, Germany) (Rink et al., 2005); mCherry-Rab5-Q79L was a gift from Sergio Grinstein (Bohdanowicz et al., 2012) (Addgene plasmid # 35138); DsRed-Rab11-S25N was a gift from Richard Pagano (Choudhury et al., 2002) (Addgene plasmid # 12680). Rab7 and Rab7-Q76L were cloned in in a pEGFP-C1 (Takara Clontech) by SmaI blunt digestion (EGFP-Rab7-WT and EGFP-Rab7-Q76L, respectively). The plasmids will be made available upon request. If the

number of requests is high enough, those plasmids will be added to a public repository (e.g. Addgene).

Immunofluorescence and antibodies

For immunofluorescence, cells were fixed for 15 min at room temperature with 3% paraformaldehyde (Electron Microscopy Sciences), washed in PBS and permeabilized with 0.05% saponin in PBS supplemented with 2 mg/mL of BSA. Coverslips were mounted in Mowiol (Calbiochem). Cell surface staining were performed with the primary antibody added in ice-cold PBS on non-fixed cells during 40 min as previously described (Boncompain and Perez, 2012). Cells were then fixed for 10 min with 2% paraformaldehyde. The mouse monoclonal anti-GFP antibody was purchased from Roche (Roche Cat# 11814460001, RRID:AB_390913; 1:300). The rabbit polyclonal Anti-Eph receptor A2+A3+A4 (phospho Y588 + Y596) antibody was purchased from abcam (Abcam Cat# ab62256, RRID:AB_942240; 1:500). The mouse monoclonal anti-LAMP1 antibody was purchased from Santa Cruz (Santa Cruz Biotechnology Cat# sc-20011, RRID:AB_626853; 1:500). The rabbit polyclonal anti-GFP (1:400), the mouse monoclonal Anti-phosphotyrosine (clone 4G10; 1:500) and the human monoclonal anti-giantin (clone TA10; 1:100) antibodies were obtained from the Recombinant Antibodies Platform (Institut Curie). Fluorescent-conjugated secondary antibodies were obtained from Jackson ImmunoResearch. SiR-DNA, SiR-Actin and SiR-Lysosome probes were purchased from Spirochrome, phalloidin-FITC was purchased from Sigma. Fixed cells were imaged with an epifluorescence microscope (Leica) equipped with a Coolsnap camera (Roper Scientific).

Live-cell imaging

Cells were seeded onto glass coverslips of 25 mm of diameter. Before imaging, coverslips were transferred into L-shape tubing Chamlide chamber (Live Cell Instrument). Chambers were filled with Leibovitz's medium (Life Technologies) pre-warmed at 37°C. For trafficking synchronization, the medium was removed and D-biotin (Sigma-Aldrich) at 40 µM in Leibovitz's medium was introduced using the tubing system of the chamber. Time-

lapse imaging were obtained in a thermostat-controlled chamber at 37°C with an Eclipse 80i microscope (Nikon) equipped with a spinning disk confocal head (Perkin) and an Ultra897 iXon camera (Andor). Image acquisitions were performed using MetaMorph software (Molecular Device) on workstations of the PICT-IBiSA Lhomond Imaging facility of Institut Curie.

Treatments

Cells seeded on coverslips were pre-treated for 1 h at 37°C with either 0.5 μM Cytochalasin D (Sigma-Aldrich), 0.5 μM Latrunculin A (Interchim), 50 μM TAPI-1 (Calbiochem), 20 μM GI254023X (Tocris Bioscience), 2.5 μM Dasatinib (Cell Signaling Technology) or DMSO (Sigma-Aldrich) as a control. The trafficking of the reporters was synchronized by addition of biotin (40 μM at 37°C) in the presence of the respective drugs. For the Cytochalasin D and Latrunculin A treatments, we corroborated the disruption of the actin microfilaments by assessing the SiR-Actin staining (0.5 μM, 1 h at 37°C). For TAPI-1 and GI254023X, the inhibition of ADAM metalloprotease was corroborated by using the SBP-Cherry-2XADAMtide-ephrin-A1-EGFP-GPI sensor. Inhibition of EphA2 signaling with Dasatinib was controlled by performing a pEphA immuno-staining.

To assure that dynamin-dependent endocytosis was inhibited after Dyngo4A (Abcam) treatment, we checked for transferrin internalization. Briefly, cells seeded on coverslips were washed 3 times with PBS and starved from serum during 5 h at 37°C in DMEM supplemented with 0.1% BSA and penicillin/streptomycin (DMEM-BSA). Cells were then pre-treated with 10 μM Dyngo4A or DMSO (Control) for 1h at 37°C in DMEM-BSA. The following incubation and washing steps were performed with DMEM-BSA containing either DMSO or 10 μM Dyngo4A. The trafficking of SBP-EGFP-ephrin-A1 was synchronized by addition of biotin (40 μM, 90 min at 37°C). Cells were then incubated for 10 min on ice with 50 μg/mL Transferrin Alexa Fluor™ 647 conjugate (Tfr-647, Molecular Probes) and washed 3 times with cold DMEM-BSA to remove the unbound Tfr-647. Transferrin internalization was allowed by incubating the cells for 10 min at 37°C. Cells were then washed 3 times with DMEM-BSA and the remnant surface-bound Tfr-647 was

stripped out by an acidic wash with Glycine buffer (0.1 M Glycine + 150 mM NaCl, pH 2.5, 30-40 sec). Finally, cells were washed in PBS, fixed with 3% PFA and mounted for imaging.

Degradative properties of the lysosomes were assessed by incubating the cells with DQ^{TM}-Green-BSA (10 μg/mL at 37°C) (ThermoFisher Scientific). Acidic lysosomes were visualized by treating cells with 75 nM LysoTracker Blue DND-22 (Invitrogen) at 37°C and imaging them live for 5 min.

Arrest of the cell cycle at G2/M border was performed by treating the cells with 9 μM RO3306 (Sigma-Aldrich) for 20 h at 37°C (Vassilev et al., 2006).

Cell confrontation assay

Cell confrontation assays were performed using cell culture inserts and 35 mm-High plates from Ibidi (Ibidi GmbH) following the instructions of the manufacturer as previously described (Porazinski et al., 2016). Cell dyes were used for better visualization; MDA-SBP-Cherry-ephrin-A1 or MDA-SBP-EGFP-EphA2 cells were labeled in suspension with Cell Proliferation Dye eFluor® 670 or 5-(and 6)-Carboxyfluorescein diacetate succinimidyl ester (CFSE-Cell Proliferation Dye) (Invitrogen), respectively (5 μM, 10 min at 37°C). The labeling was stopped by incubating the cells with ice-cold DMEM medium supplemented with 20% FCS during 5 min, followed of three washes with 20% FCS medium (5 min, 1200 x g each). 3-4 x 10^4 cells were then seeded into each compartment of the insert and incubated in presence of 80 μM of D-biotin at 37°C for 12-20 h before the removal of the insert. Upon reaching confluence, the insert was removed. Non-adhered cells were gently washed out with PBS and the dish was filled with 2 mL of 80 μM D-biotin-containing DMEM. 8-12 h after insert removal the medium was switched to Leibovitz's medium

supplemented with 80 μM of D-biotin and 10% FBS. The cells were imaged-live using a spinning disk confocal microscope with a 20X objective.

Co-culture assay

HeLa cells were first electroporated with the appropriate plasmid and then mixed. Electroporation were performed using the NEPA21 system (Nepa Gene Co.) according to the manufacturer's instructions. Briefly, cells were electroporated in Opti-MEM medium (Invitrogen) supplemented with 7 μg/mL of avidin (Sigma-Aldrich) to neutralize the traces of biotin present in the medium. 1 x 10^6 of HeLa cells in suspension were mixed with 10 μg of DNA up to a final volume of 100 μL. For the electroporation of mRFP-Rab5-WT, mCherry-Rab5-Q79L, EGFP-Rab11-WT, DsRed-Rab11-S25N, EGFP-Rab7-WT and EGFP-Rab7-Q76L, 5μg of each plasmid were mixed with 5μg of an empty vector. Cells were then transferred to 2 mm gap cuvettes and electroporated using 2 poring pulses of 125 V, 7.5 msec length and 50 msec interval, followed by 5 transfer pulses of 20 V, 50 msec length and 50 msec interval. Equal amounts of donor and acceptor cells were then seeded onto 35 mm coverslip with pre-warmed medium and mixed by pipetting until a mono-disperse cell suspension was achieved. Before imaging, cells were gently washed 3 times with PBS to remove dead cells and debris.

Ephrin inheritance assay

Wild-type MDA-MB231 cells (acceptor) were labeled in suspension with CFSE-Cell Proliferation Dye and seeded on gridded 35 mm-High plates from Ibidi (Ibidi GmbH) following the instructions of the manufacturer. After 24h the cell cycle was arrested at G2/M transition using the reversible CDK1 inhibitor RO3306 (9 μM, 20 h at 37°C) (Vassilev et al., 2006). Then HeLa-SBP-Cherry-ephrin-A1 cells (donor) were seeded on top of the monolayer of acceptor cells and were let adhere in the presence of 40 μM D-biotin-containing DMEM for 2-4 h before imaging. The imaging field were chosen and the coordinates of the grid were registered. Then the cells were washed 5 times for 1 min with Leibovitz's medium and imaged live using a spinning disk confocal microscopy with a 63X

objective as described before. After completion of mitosis, the cells were fixed for 15 min at room temperature with 3% paraformaldehyde and processed for immunofluorescence with antibodies against LAMP1 and pEphA receptors. The cells were located using the coordinates on the gridded plate and imaged using the same microscope and objective as above. Images were then manually aligned using Fiji software.

QUANTIFICATION AND STATISTICAL ANALYSIS

Image quantification

Normalized Golgi intensity was obtained by measuring the integrated intensity over the time in a mask of the Golgi apparatus, whose position was determined from latter time points as previously described (Boncompain et al., 2012). The same mask was then positioned in a cell-free region (background) and the integrated intensity over the time was measured and subtracted to the integrated Golgi intensity. The values were normalized to the maximal value, and the measurements before the addition of biotin were adjusted to zero.

Colocalization percentages over the time were determined in background subtracted cropped images containing individual cells. Single channel masks were generated by thresholding of each channel. The colocalization area was measured and normalized to the total area of each channel for every time point. The values were then translated in percentages. Random colocalization was determined by displacing the red channel 5x5 pixels in the *xy* plane for all the time points.

The start of clustering and secretion were determined by visual inspection of videos of cells co-transfected with the RUSH reporter SBP-EGFP-ephrin-A1 and PM-Cherry to delimit the donor cell. The start of clustering was considered as the time point at which the first bright ephrin-A1 structure appeared at the PM of a given cell before to be exported. The start of the secretion was stated as the time point at which the first ephrin-A1 cluster was distinguishable separated from the PM of its donor cell. The normalized number of

transferred clusters was extracted from fixed epifluorescence images acquired with a 63X objective. The total number of exported clusters in each field was determined by manual counting and multiplied by the ratio of donor / acceptor cells.

For lysosomes-related quantifications, we measured the integrated intensity and area of hand-drawn region of interests (ROIs) comprising ephrin-A1-containing lysosomes, ephrin-A1-negative lysosomes or cytosolic lysosomes-free ROIs of the same size. For the cell confrontation assays we determined the distance traveled by the marginal cells after collision by measuring the distance between two parallels lines depicting the point of the first cell-to-cell contact and the position of the front of migration 20 h after this contact respectively. All these quantifications were made using Fiji software (Schindelin et al., 2012) and Microsoft® Excel® 14.7.1 for drawing the plots. For boxplots; boxes represent 25^{th} and 75^{th} percentiles, the whiskers extend to the most extreme data points and the median is indicated as a band inside the box. The data were compared by using the two-tailed t-test.

DATA AND CODE AVAILABILITY

This study did not generate/analyze datasets or codes

Additional information

SUPPLEMENTARY INFORMATION

Correspondence and request for materials should be addressed to J.I.V. or F.P.

SUPPLEMENTARY VIDEOS

Supplementary Video 1 (Related to Figure 1) Partial sorting of EphA2 and ephrin-A1 at the Golgi apparatus

Supplementary Video 2 (Related to Figure 1) Ephrin-A1 is exported from filopodia of ligand-producing cells

Supplementary Video 3 (Related to Figure 2) Ephrin-A5 is transferred to neighboring cells from filopodia

Supplementary Video 5 (Related to Figure 2) Actin-dependent trans-endocytosis of ephrin-A1 from filopodia

Supplementary Video 6 (Related to Figure 3) Cleavage-independent trans-endocytosis of ephrin-A1

Supplementary Video 7 (Related to Figure 4) Dynamin-dependent trans-endocytosis of ephrin-A1

Supplementary Video 8 (Related to Figure 5) Localized trans-endocytosis of ephrin-A1/EphA2 complexes

Supplementary Video 9 (Related to Figure 5) Trans-endocytosis of ephrin-A1 is massive at steady state

Supplementary Video 10 (Related to Figure 7) Inheritance of trans-endocytosed ephrin-A1 in cancer cells

SUPPLEMENTARY FIGURES

Supplementary Figure 1 Synthetic sensor of ADAM protease-based trans-endocytosis of ephrin-A1 (Related to Figure 3)

(A) Scheme of the experimental design of the ADAM-cleavage sensor SBP-Cherry-2XADAMtide-ephrin-A1-EGFP-GPI. The blue fragment represents the position of the inserted repetitions (2x) of the consensus ADAM cleavage site (ADAMtide).

(B) Time-lapse imaging of HeLa cells transfected with the SBP-Cherry-2XADAMtide-ephrin-A1-EGFP-GPI sensor. EGFP and Cherry signals are shown. Cell-cell boundaries are visualized with the actin probe SiR-Actin (blue). Bottom panels (high-magnification images of a donor/acceptor cell interface).

(C) Kymograph analysis of one cluster of SBP-Cherry-2XADAMtide-ephrin-A1-EGFP-GPI into an acceptor cell.

(D) Line-scan analysis and EGFP/Cherry intensity ratio obtained from the kymograph in (C).

(E-G) Same as in (B-D), but for cells treated with the metalloprotease's inhibitor TAPI-1.

(H-J) Same as in (B-D), but for cells treated with the ADAM-10 inhibitor GI254023X. Scale bars, 10 μm.

Supplementary Figure 2 Trans-endocytosed ephrin-A1 is sorted apart from Rab11-recycling endosomes (Related to Figure 4)

(A) Time-lapse imaging of HeLa cells expressing SBP-Cherry-ephrin-A1 co-cultured with cells expressing EGFP-Rab11-WT. Single channels are shown in inverted colors for better visualization (ephrin-A1 in the top row and Rab11 in the middle row). Merge images are shown (bottom panels: ephrin-A1, red; Rab11, green). Cell-cell interfaces were visualized by the SiR-Actin labeling (blue). Arrows indicate an example of trans-endocytosed SBP-Cherry-ephrin-A1 cluster in an acceptor cell.

(B) Same as in (A) but for cells expressing SBP-EGFP-ephrin-A1 (top row) and co-cultured with cells expressing DsRED-Rab11-S25N mutant (middle row). Scale bars, 10 μm.

Supplementary Figure 3 Activation of EphA receptors at the plasma membrane is necessary for ephrin-A1 trans-endocytosis (Related to Figure 5)

(A) HeLa cells expressing SBP-EGFP-ephrin-A1 (green) were co-cultured with HeLa cells expressing Dynamin-I-WT-CFP (blue, top panels) or Dynamin-I-K44A-CFP (blue, bottom panels). Cells were treated with biotin (90 min), fixed and stained with an antibody against active phosphorylated EphA receptors (pEphA, red). Right panels show high-magnification

images of the boxed area. Arrows indicate examples of trans-endocytosed SBP-EGFP-ephrin-A1 clusters in an acceptor cell co-localizing with active EphA receptors.

(B) HeLa cells co-expressing SBP-Cherry-ephrin-A1 (red) and PM-EGFP (blue), under control conditions (upper panels) or after EphA2 signaling inhibition with Dasatinib (bottom panels). Cells were fixed after 90 min of biotin addition. Immuno-staining with an antibody against active phosphorylated EphA receptors (pEphA, green) are shown. Right panels show high-magnification images of donor/acceptor cell interfaces (boxed area in the left panel). Arrows indicate examples of trans-endocytosed SBP-Cherry-ephrin-A1 clusters in an acceptor cell co-localizing with active EphA receptors. PM-EGFP is show in inverted colors (right panels) to highlight the long donor filopodia inside the acceptor cell after EphA receptor inhibition. Scale bars, 10 μm.

Supplementary Figure 4 Trans-endocytosed ephrin-A1 is co-transported with EphA2 and stored for a long time in acidic lysosomes in MDA-MB231 cells (Related to Figure 6)

(A) Live-cell imaging of MDA-MB231 cells stably expressing the RUSH construct SBP-Cherry-ephrin-A1 (SBP-Cherry-ephrin-A1, red) co-cultured with MDA-MB231 cells expressing steady-state SBP-EGFP-EphA2 (SBP-EGFP-EphA2 in the absence of hook expression, green). Lysosomes were stained with the SiR-lysosome dye (blue). High-magnification images are presented below in black and white: SBP-Cherry-ephrin-A1 (top row), SBP-EGFP-EphA2 (middle-upper row) and SiR-lysosome (middle-lower row).

Merge images are shown (bottom row). Arrows indicate an example of a trans-endocytosed SBP-Cherry-ephrin-A1 cluster co-transported with SBP-EGFP-EphA2 towards a large lysosomal structure in an acceptor cell.

(B) Single frame from live-cell imaging of MDA-MB231 cells stably expressing the RUSH construct SBP-Cherry-ephrin-A1 (SBP-Cherry-ephrin-A1, red) co-cultured with wild-type MDA-MB231 cells (left pannel). High magnification images of an acceptor cell are shown. Right panels shown the same cell after a short treatment with the acidotrophic dye Lysotracker (blue). Arrows indicate trans-endocytosed SBP-Cherry-ephrin-A1 in acidic lysosomes.

(C) Live-cell imaging of MDA-MB231 cells stably expressing the RUSH construct SBP-Cherry-ephrin-A1 (SBP-Cherry-ephrin-A1, red) co-cultured with wild-type MDA-MB231 cells. Lysosomes were stained with the SiR-lysosome dye (blue). Degradative compartements were detected by the fluorogenic protease substrate DQ-BSA (green). High-magnification images are presented below in black and white: SBP-Cherry-ephrin-A1 (top row), DQ-BSA (middle-upper row) and SiR-lysosome (middle-lower row). Merge images are shown (bottom row). Arrows indicate trans-endocytosed SBP-Cherry-ephrin-A1 in degradative lysosomes. Scale bars, 10 μm.

References

Abounit, S., Bousset, L., Loria, F., Zhu, S., de Chaumont, F., Pieri, L., Olivo-Marin, J.-C., Melki, R., and Zurzolo, C. (2016). Tunneling nanotubes spread fibrillar α-synuclein by intercellular trafficking of lysosomes. EMBO J. *35*, 2120–2138.

Barquilla, A., and Pasquale, E.B. (2015). Eph receptors and ephrins: therapeutic opportunities. Annu. Rev. Pharmacol. Toxicol. *55*, 465–487.

Batlle, E., and Wilkinson, D.G. (2012). Molecular mechanisms of cell segregation and boundary formation in development and tumorigenesis. Cold Spring Harb. Perspect. Biol. *4*, a008227.

Beauchamp, a., Lively, M.O., Mintz, A., Gibo, D., Wykosky, J., and Debinski, W. (2012). EphrinA1 Is Released in Three Forms from Cancer Cells by Matrix Metalloproteases. Mol. Cell. Biol. *32*, 3253–3264.

Belin, B.J., Goins, L.M., and Mullins, R.D. (2014). Comparative analysis of tools for live cell imaging of actin network architecture. Bioarchitecture *4*, 189–202.

Bergeland, T., Widerberg, J., Bakke, O., and Nordeng, T.W. (2001). Mitotic partitioning of endosomes and lysosomes. Curr. Biol. *11*, 644–651.

Bohdanowicz, M., Balkin, D.M., De Camilli, P., and Grinstein, S. (2012). Recruitment of OCRL and Inpp5B to phagosomes by Rab5 and APPL1 depletes phosphoinositides and attenuates Akt signaling. Mol. Biol. Cell *23*, 176–187.

Boncompain, G., and Perez, F. (2012). Synchronizing protein transport in the secretory pathway. Curr. Protoc. Cell Biol. 1–16.

Boncompain, G., Divoux, S., Gareil, N., de Forges, H., Lescure, A., Latreche, L., Mercanti, V., Jollivet, F., Raposo, G., and Perez, F. (2012). Synchronization of secretory protein traffic in populations of cells. Nat. Methods *9*, 493–498.

Boyd, A.W., Bartlett, P.F., and Lackmann, M. (2014). Therapeutic targeting of EPH

909 receptors and their ligands. Nat. Rev. Drug Discov. *13*, 39–62.

910 Burtey, A., Wagner, M., Hodneland, E., Skaftnesmo, K.O., Schoelermann, J.,
911 Mondragon, I.R., Espedal, H., Golebiewska, A., Niclou, S.P., Bjerkvig, R., et al. (2015).
912 Intercellular transfer of transferrin receptor by a contact-, Rab8-dependent
913 mechanism involving tunneling nanotubes. FASEB J. *29*, 4695–4712.

914 Caescu, C.I., Jeschke, G.R., and Turk, B.E. (2009). Active-site determinants of
915 substrate recognition by the metalloproteinases TACE and ADAM10. Biochem. J. *424*,
916 79–88.

917 Cayuso, J., Dzementsei, A., Fischer, J.C., Karemore, G., Caviglia, S., Bartholdson, J.,
918 Wright, G.J., and Ober, E.A. (2016). EphrinB1/EphB3b Coordinate Bidirectional
919 Epithelial-Mesenchymal Interactions Controlling Liver Morphogenesis and
920 Laterality. Dev. Cell *39*, 316–328.

921 Chang, Q., Jorgensen, C., Pawson, T., and Hedley, D.W. (2008). Effects of dasatinib on
922 EphA2 receptor tyrosine kinase activity and downstream signalling in pancreatic
923 cancer. Br. J. Cancer *99*, 1074–1082.

924 Choudhury, A., Dominguez, M., Puri, V., Sharma, D.K., Narita, K., Wheatley, C.L., Marks,
925 D.L., and Pagano, R.E. (2002). Rab proteins mediate Golgi transport of caveola-
926 internalized glycosphingolipids and correct lipid trafficking in Niemann-Pick C cells.
927 J. Clin. Invest. *109*, 1541–1550.

928 Connor, Y., Tekleab, S., Nandakumar, S., Walls, C., Tekleab, Y., Husain, A., Gadish, O.,
929 Sabbisetti, V., Kaushik, S., Sehrawat, S., et al. (2015). Physical nanoscale conduit-
930 mediated communication between tumour cells and the endothelium modulates
931 endothelial phenotype. Nat. Commun. *6*, 8671.

932 Davis, S., Gale, N.W., Aldrich, T.H., Maisonpierre, P.C., Lhotak, V., Pawson, T., Goldfarb,
933 M., and Yancopoulos, G.D. (1994). Ligands for EPH-related receptor tyrosine kinases
934 that require membrane attachment or clustering for activity. Science *266*, 816–819.

Fiore, L., Medori, M., Spelzini, G., Carreño, C.O., Carri, N.G., Sanchez, V., and Scicolone, G. (2019). Regulation of axonal EphA4 forward signaling is involved in the effect of EphA3 on chicken retinal ganglion cell axon growth during retinotectal mapping. Exp. Eye Res. *178*, 46–60.

Fourriere, L., Kasri, A., Gareil, N., Bardin, S., Bousquet, H., Pereira, D., Perez, F., Goud, B., Boncompain, G., and Miserey-Lenkei, S. (2019). RAB6 and microtubules restrict protein secretion to focal adhesions. J. Cell Biol. *218*, 2215–2231.

Gaitanos, T.N., Koerner, J., and Klein, R. (2016). Tiam-Rac signaling mediates trans-endocytosis of ephrin receptor EphB2 and is important for cell repulsion. J. Cell Biol. *214*, 735–752.

Georgakopoulos, A., Litterst, C., Ghersi, E., Baki, L., Xu, C., Serban, G., and Robakis, N.K. (2006). Metalloproteinase/Presenilin1 processing of ephrinB regulates EphB-induced Src phosphorylation and signaling. EMBO J. *25*, 1242–1252.

Gong, J., Körner, R., Gaitanos, L., and Klein, R. (2016). Exosomes mediate cell contact-independent ephrin-Eph signaling during axon guidance. J. Cell Biol. *214*, 35–44.

Gong, J., Gaitanos, T.N., Luu, O., Huang, Y., Gaitanos, L., Lindner, J., Winklbauer, R., and Klein, R. (2019). Gulp1 controls Eph/ephrin trogocytosis and is important for cell rearrangements during development. J. Cell Biol.

Gousset, K., Schiff, E., Langevin, C., Marijanovic, Z., Caputo, A., Browman, D.T., Chenouard, N., de Chaumont, F., Martino, A., Enninga, J., et al. (2009). Prions hijack tunnelling nanotubes for intercellular spread. Nat. Cell Biol. *11*, 328–336.

Greene, A.C., Lord, S.J., Tian, A., Rhodes, C., Kai, H., and Groves, J.T. (2014). Spatial organization of EphA2 at the cell-cell interface modulates trans-endocytosis of ephrinA1. Biophys. J. *106*, 2196–2205.

Hattori, M., Osterfield, M., and Flanagan, J.G. (2000). Regulated cleavage of a contact-mediated axon repellent. Science *289*, 1360–1365.

961 Ieguchi, K., Tomita, T., Omori, T., Komatsu, A., Deguchi, A., Masuda, J., Duffy, S.L.,
962 Coulthard, M.G., Boyd, A., and Maru, Y. (2014). ADAM12-cleaved ephrin-A1
963 contributes to lung metastasis. Oncogene *33*, 2179–2190.

964 Janes, P.W., Saha, N., Barton, W.A., Kolev, M. V., Wimmer-Kleikamp, S.H., Nievergall,
965 E., Blobel, C.P., Himanen, J.P., Lackmann, M., and Nikolov, D.B. (2005). Adam meets
966 Eph: An ADAM substrate recognition module acts as a molecular switch for ephrin
967 cleavage in trans. Cell *123*, 291–304.

968 Janes, P.W., Wimmer-Kleikamp, S.H., Frangakis, A.S., Treble, K., Griesshaber, B., Sabet,
969 O., Grabenbauer, M., Ting, A.Y., Saftig, P., Bastiaens, P.I., et al. (2009). Cytoplasmic
970 relaxation of active Eph controls ephrin shedding by ADAM10. PLoS Biol. *7*,
971 e1000215.

972 Johannessen, C.M., Boehm, J.S., Kim, S.Y., Thomas, S.R., Wardwell, L., Johnson, L.A.,
973 Emery, C.M., Stransky, N., Cogdill, A.P., Barretina, J., et al. (2010). COT drives
974 resistance to RAF inhibition through MAP kinase pathway reactivation. Nature *468*,
975 968–972.

976 Jordan, M., Schallhorn, A., and Wurm, F.M. (1996). Transfecting mammalian cells:
977 optimization of critical parameters affecting calcium-phosphate precipitate
978 formation. Nucleic Acids Res. *24*, 596–601.

979 Jurney, W.M., Gallo, G., Letourneau, P.C., and McLoon, S.C. (2002). Rac1-mediated
980 endocytosis during ephrin-A2- and semaphorin 3A-induced growth cone collapse. J.
981 Neurosci. *22*, 6019–6028.

982 Kania, A., and Klein, R. (2016). Mechanisms of ephrin-Eph signalling in development,
983 physiology and disease. Nat. Rev. Mol. Cell Biol. *17*, 240–256.

984 Kaplan, N., Ventrella, R., Peng, H., Pal-Ghosh, S., Arvanitis, C., Rappoport, J.Z., Mitchell,
985 B.J., Stepp, M.A., Lavker, R.M., and Getsios, S. (2018). EphA2/Ephrin-A1 Mediate
986 Corneal Epithelial Cell Compartmentalization via ADAM10 Regulation of EGFR

Signaling. Invest. Ophthalmol. Vis. Sci. *59*, 393–406.

Klein, R. (2009). Bidirectional modulation of synaptic functions by Eph/ephrin signaling. Nat. Neurosci. *12*, 15–20.

Koizumi, K., Takano, K., Kaneyasu, A., Watanabe-Takano, H., Tokuda, E., Abe, T., Watanabe, N., Takenawa, T., and Endo, T. (2012). RhoD activated by fibroblast growth factor induces cytoneme-like cellular protrusions through mDia3C. Mol. Biol. Cell *23*, 4647–4661.

Kornberg, T.B., and Roy, S. (2014). Communicating by touch – neurons are not alone. Trends Cell Biol. *24*, 370–376.

Krupke, O.A., Zysk, I., Mellott, D.O., and Burke, R.D. (2016). Eph and Ephrin function in dispersal and epithelial insertion of pigmented immunocytes in sea urchin embryos. Elife *5*.

Lidke, D.S., Lidke, K.A., Rieger, B., Jovin, T.M., and Arndt-Jovin, D.J. (2005). Reaching out for signals: filopodia sense EGF and respond by directed retrograde transport of activated receptors. J. Cell Biol. *170*, 619–626.

Litterst, C., Georgakopoulos, A., Shioi, J., Ghersi, E., Wisniewski, T., Wang, R., Ludwig, A., and Robakis, N.K. (2007). Ligand binding and calcium influx induce distinct ectodomain/gamma-secretase-processing pathways of EphB2 receptor. J. Biol. Chem. *282*, 16155–16163.

Lu, M., Miller, K.D., Gokmen-Polar, Y., Jeng, M.-H., and Kinch, M.S. (2003). EphA2 overexpression decreases estrogen dependence and tamoxifen sensitivity. Cancer Res. *63*, 3425–3429.

Marston, D.J., Dickinson, S., and Nobes, C.D. (2003). Rac-dependent trans-endocytosis of ephrinBs regulates Eph-ephrin contact repulsion. Nat. Cell Biol. *5*, 879–888.

Moti, N., Yu, J., Boncompain, G., Perez, F., and Virshup, D.M. (2019). Wnt traffic from endoplasmic reticulum to filopodia. PLoS One *14*, e0212711.

Osswald, M., Jung, E., Sahm, F., Solecki, G., Venkataramani, V., Blaes, J., Weil, S., Horstmann, H., Wiestler, B., Syed, M., et al. (2015). Brain tumour cells interconnect to a functional and resistant network. Nature *528*, 93–98.

Pasquale, E.B. (2008). Eph-Ephrin Bidirectional Signaling in Physiology and Disease. Cell *133*, 38–52.

Porazinski, S., de Navascués, J., Yako, Y., Hill, W., Jones, M.R., Maddison, R., Fujita, Y., Hogan, C., Anton, K.A., Sinclair, J., et al. (2016). EphA2 Drives the Segregation of Ras-Transformed Epithelial Cells from Normal Neighbors. Curr. Biol. *26*, 3220–3229.

Prospéri, M.-T., Lépine, P., Dingli, F., Paul-Gilloteaux, P., Martin, R., Loew, D., Knölker, H.-J., and Coudrier, E. (2015). Myosin 1b functions as an effector of EphB signaling to control cell repulsion. J. Cell Biol. *210*, 347–361.

Rink, J., Ghigo, E., Kalaidzidis, Y., and Zerial, M. (2005). Rab conversion as a mechanism of progression from early to late endosomes. Cell *122*, 735–749.

Sabet, O., Stockert, R., Xouri, G., Brüggemann, Y., Stanoev, A., and Bastiaens, P.I.H. (2015). Ubiquitination switches EphA2 vesicular traffic from a continuous safeguard to a finite signalling mode. Nat. Commun. *6*, 8047.

Schaupp, A., Sabet, O., Dudanova, I., Ponserre, M., Bastiaens, P., and Klein, R. (2014). The composition of EphB2 clusters determines the strength in the cellular repulsion response. J. Cell Biol. *204*, 409–422.

Schindelin, J., Arganda-Carreras, I., Frise, E., Kaynig, V., Longair, M., Pietzsch, T., Preibisch, S., Rueden, C., Saalfeld, S., Schmid, B., et al. (2012). Fiji: an open-source platform for biological-image analysis. Nat. Methods *9*, 676–682.

Seiradake, E., Schaupp, A., del Toro Ruiz, D., Kaufmann, R., Mitakidis, N., Harlos, K., Aricescu, A.R., Klein, R., and Jones, E.Y. (2013). Structurally encoded intraclass differences in EphA clusters drive distinct cell responses. Nat. Struct. Mol. Biol. *20*, 958–964.

1039 Shaw, A., Lundin, V., Petrova, E., Fördős, F., Benson, E., Al-Amin, A., Herland, A.,
1040 Blokzijl, A., Högberg, B., and Teixeira, A.I. (2014). Spatial control of membrane
1041 receptor function using ligand nanocalipers. Nat. Methods *11*, 841–846.

1042 Sherer, N.M., and Mothes, W. (2008). Cytonemes and tunneling nanotubules in cell–
1043 cell communication and viral pathogenesis. Trends Cell Biol. *18*, 414–420.

1044 Solanas, G., Cortina, C., Sevillano, M., and Batlle, E. (2011). Cleavage of E-cadherin by
1045 ADAM10 mediates epithelial cell sorting downstream of EphB signalling. Nat. Cell
1046 Biol. *13*, 1100–1107.

1047 Song, B.D., Yarar, D., and Schmid, S.L. (2004). An assembly-incompetent mutant
1048 establishes a requirement for dynamin self-assembly in clathrin-mediated
1049 endocytosis in vivo. Mol. Biol. Cell *15*, 2243–2252.

1050 Stallaert, W., Brüggemann, Y., Sabet, O., Baak, L., Gattiglio, M., and Bastiaens, P.I.H.
1051 (2018). Contact inhibitory Eph signaling suppresses EGF-promoted cell migration by
1052 decoupling EGFR activity from vesicular recycling. Sci. Signal. *11*, eaat0114.

1053 Stein, E., Lane, A.A., Cerretti, D.P., Schoecklmann, H.O., Schroff, A.D., Van Etten, R.L.,
1054 and Daniel, T.O. (1998). Eph receptors discriminate specific ligand oligomers to
1055 determine alternative signaling complexes, attachment, and assembly responses.
1056 Genes Dev. *12*, 667–678.

1057 Tomita, T., Tanaka, S., Morohashi, Y., and Iwatsubo, T. (2006). Presenilin-dependent
1058 intramembrane cleavage of ephrin-B1. Mol. Neurodegener. *1*, 2.

1059 Tremblay, M.-È., Riad, M., Chierzi, S., Murai, K.K., Pasquale, E.B., and Doucet, G.
1060 (2009). Developmental course of EphA4 cellular and subcellular localization in the
1061 postnatal rat hippocampus. J. Comp. Neurol. *512*, 798–813.

1062 Vassilev, L.T., Tovar, C., Chen, S., Knezevic, D., Zhao, X., Sun, H., Heimbrook, D.C., and
1063 Chen, L. (2006). Selective small-molecule inhibitor reveals critical mitotic functions
1064 of human CDK1. Proc. Natl. Acad. Sci. U. S. A. *103*, 10660–10665.

White, B.E.P., and Getsios, S. (2014). Eph receptor and ephrin function in breast, gut, and skin epithelia. Cell Adhes. Migr. *8*, 327–338.

Wykosky, J., and Debinski, W. (2008). The EphA2 receptor and ephrinA1 ligand in solid tumors: function and therapeutic targeting. Mol. Cancer Res. *6*, 1795–1806.

Wykosky, J., Palma, E., Gibo, D.M., Ringler, S., Turner, C.P., and Debinski, W. (2008). Soluble monomeric EphrinA1 is released from tumor cells and is a functional ligand for the EphA2 receptor. Oncogene *27*, 7260–7273.

Yoo, S., Shin, J., and Park, S. (2010). EphA8-ephrinA5 signaling and clathrin-mediated endocytosis is regulated by Tiam-1, a Rac-specific guanine nucleotide exchange factor. Mol. Cells *29*, 603–609.

Yoo, S., Kim, Y., Noh, H., Lee, H., Park, E., and Park, S. (2011). Endocytosis of EphA receptors is essential for the proper development of the retinocollicular topographic map. EMBO J. *30*, 1593–1607.

Zacharias, D.A., Violin, J.D., Newton, A.C., and Tsien, R.Y. (2002). Partitioning of lipid-modified monomeric GFPs into membrane microdomains of live cells. Science *296*, 913–916.

Zhuang, G., Hunter, S., Hwang, Y., and Chen, J. (2007). Regulation of EphA2 receptor endocytosis by SHIP2 lipid phosphatase via phosphatidylinositol 3-kinase-dependent Rac1 activation. J. Biol. Chem. *282*, 2683–2694.

Zhuang, G., Brantley-Sieders, D.M., Vaught, D., Yu, J., Xie, L., Wells, S., Jackson, D., Muraoka-Cook, R., Arteaga, C., and Chen, J. (2010). Elevation of receptor tyrosine kinase EphA2 mediates resistance to trastuzumab therapy. Cancer Res. *70*, 299–308.

Zimmer, M., Palmer, A., Köhler, J., and Klein, R. (2003). EphB-ephrinB bi-directional endocytosis terminates adhesion allowing contact mediated repulsion. Nat. Cell Biol. *5*, 869–878.

(1997). Unified nomenclature for Eph family receptors and their ligands, the

ephrins. Eph Nomenclature Committee. Cell *90*, 403–404.

TABLE FOR AUTHOR TO COMPLETE

KEY RESOURCES TABLE

REAGENT or RESOURCE	SOURCE	IDENTIFIER
Antibodies		
Mouse monoclonal anti-GFP	Roche	Cat#11814460001; RRID:AB_390913
Rabbit polyclonal Anti-Eph receptor A2+A3+A4 (phospho Y588 + Y596)	Abcam	Cat#ab62256; RRID:AB_942240
Mouse monoclonal anti-LAMP1	Santa Cruz Biotechnology	Cat#sc-20011; RRID:AB_626853
Rabbit polyclonal anti-GFP	Recombinant Antibodies Platform (Institut Curie)	A-P-R#06
Mouse monoclonal Anti-phosphotyrosine (clone 4G10)	Recombinant Antibodies Platform (Institut Curie)	A-M-M#09
Human monoclonal anti-giantin (clone TA10)	Recombinant Antibodies Platform (Institut Curie)	A-R-H#03
Bacterial and Virus Strains		
Biological Samples		
Chemicals, Peptides, and Recombinant Proteins		
Avidin	Sigma-Aldrich	Cat#A-9275
Cell Proliferation Dye eFluor® 670	Invitrogen	Cat#65-0840-90
5-(and 6)-Carboxyfluorescein diacetate succinimidyl ester (CFSE-Cell Proliferation Dye)	Sigma-Aldrich	Cat#21888
Cytochalasin D	Sigma-Aldrich	Cat#C8273
Dasatinib	Cell Signaling Technology	Cat#9052S
D-biotin	Sigma-Aldrich	Cat#B4501
DMSO	Sigma-Aldrich	Cat#D2438
DQ™-Green-BSA	ThermoFisher Scientific	Cat#D12050
Dyngo4A	Abcam	Cat#Ab120689
GI254023X	Tocris Bioscience	Cat#3995
Latrunculin A	Interchim	Cat#L-12370
LysoTracker Blue DND-22	Invitrogen	Cat#L7525
Phalloidin-FITC	Sigma-Aldrich	Cat#P5282

RO3306	Sigma-Aldrich	Cat#SML0569
SiR-Actin	Spirochrome	Cat#SC001
SiR-DNA	Spirochrome	Cat#SC007
SiR-Lysosome	Spirochrome	Cat#SC012
TAPI-1	Tocris Bioscience	Cat#6162
Transferrin Alexa FluorTM 647	Molecular Probes	Cat#T23366
Critical Commercial Assays		
Culture-Insert 3 Well in μ-Dish 35 mm, high	Ibidi	Cat#80366
Deposited Data		
Experimental Models: Cell Lines		
Human: HeLa	ATCC	ATCC CCL-2
Human: MDA-MB-231	ATCC	ATCC HTB-26
Experimental Models: Organisms/Strains		
Oligonucleotides		
Recombinant DNA		
pmCherry-C1	Clontech	Cat#632524
pEGFP-C1	Clontech	This plasmid has been discontinued
pCDH-CMV-MCS-EF1α-Puro	System Biosciences	Cat#CD510B-1
Dynamin-1-WT-EGFP	(Song et al., 2004)	Addgene plasmid #34680
Dynamin-1-K44A-EGFP	(Song et al., 2004)	Addgene plasmid #34681
F-tractin-EGFP	(Belin et al., 2014)	Addgene plasmid #58473

pDONR223-EPHA2	(Johannessen et al., 2010)	Addgene plasmid #23926
DsRed-Rab11-S25N	(Choudhury et al., 2002)	Addgene plasmid # 12680
SBP-Cherry-GPI	(Boncompain et al., 2012)	Addgene plasmid #65295
PM-EGFP	(Zacharias et al., 2002)	N/A
mRFP-Rab5-WT	(Rink et al., 2005)	N/A
SBP-Cherry-ALPP	(Fourriere et al., 2019)	N/A
SBP-Cherry-CD59	(Fourriere et al., 2019)	N/A
EGFP-Rab7-WT	This paper	N/A
EGFP-Rab7-Q76L	This paper	N/A
Dynamin-1-WT-CFP	This paper	N/A
Dynamin-1-K44A-CFP	This paper	N/A
PM-Cherry	This paper	N/A
SBP-EGFP-ephrin-A1	This paper	N/A
SBP-Cherry-ephrin-A1	This paper	N/A
SBP-EGFP-ephrin-A5	This paper	N/A
SBP-EGFP-EphA2	This paper	N/A
EphA2-EGFP-SBP	This paper	N/A
EphA2-Cherry-SBP	This paper	N/A
SBP-Cherry-ephrin-A1-EGFP-GPI	This paper	N/A
SBP-Cherry-ephrin-A1-TMD-ephrin-B1-EGFP	This paper	N/A
SBP-Cherry-2xADAMtide-ephrin-A1-EGFP-GPI	This paper	N/A
Software and Algorithms		
Fiji	(Schindelin et al., 2012)	https://fiji.sc/
MetaMorph software	Molecular Device	
Other		

Figure 1

Click here to access/download;Figure;Figure1.tif

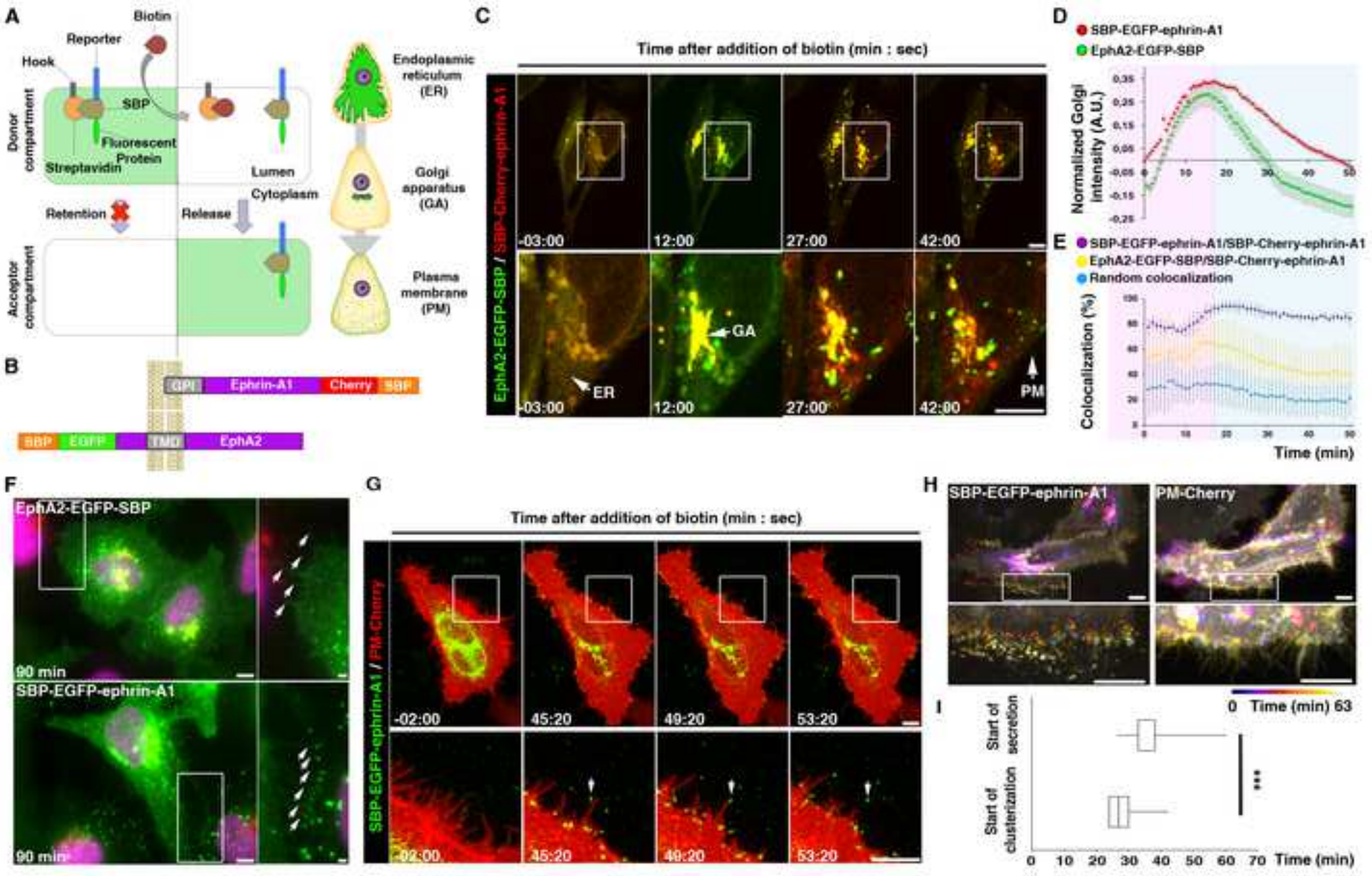

Figure 2

Click here to access/download;Figure;Figure2.tif

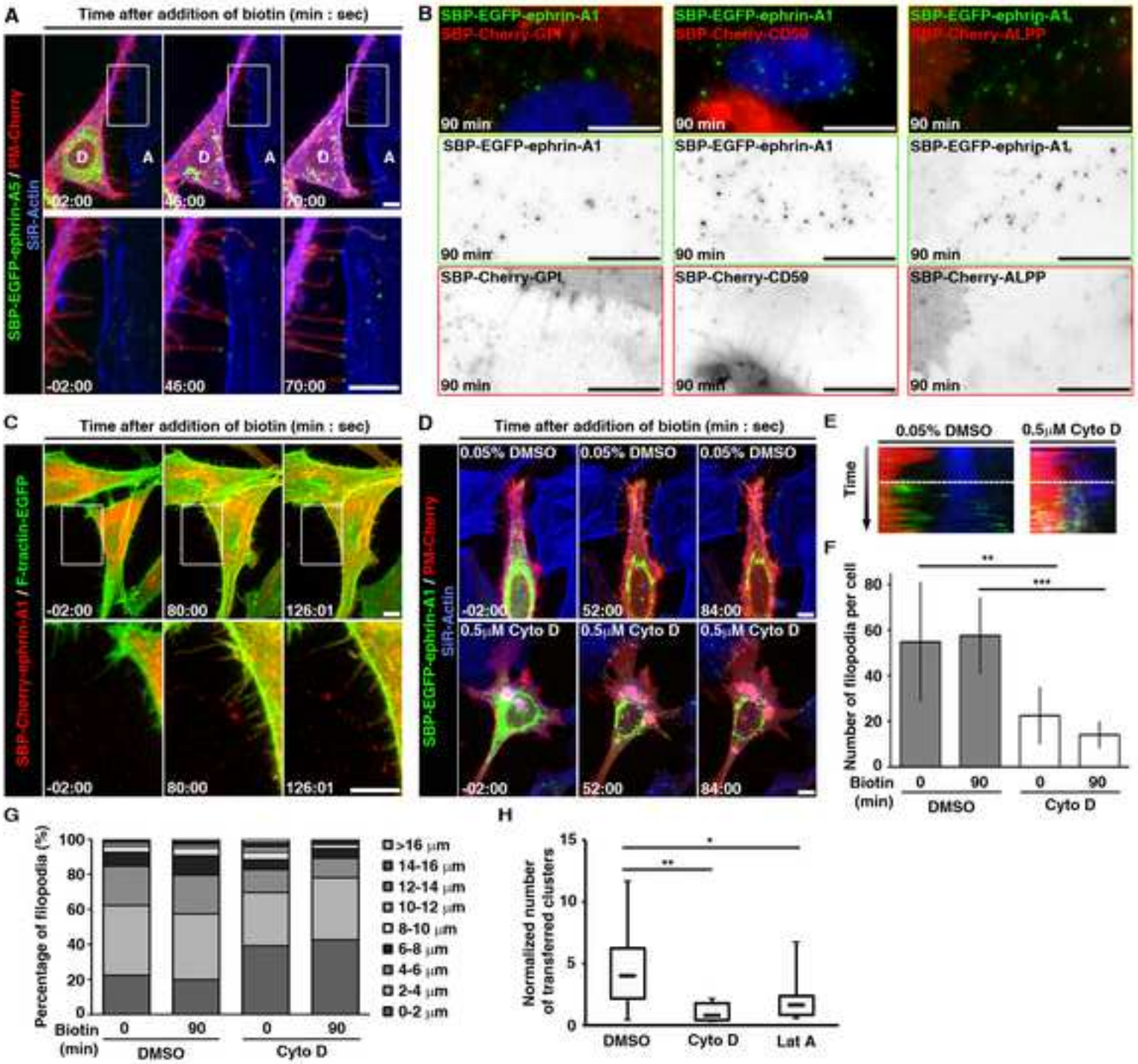

Figure 3

Click here to access/download;Figure;Figure3.tif

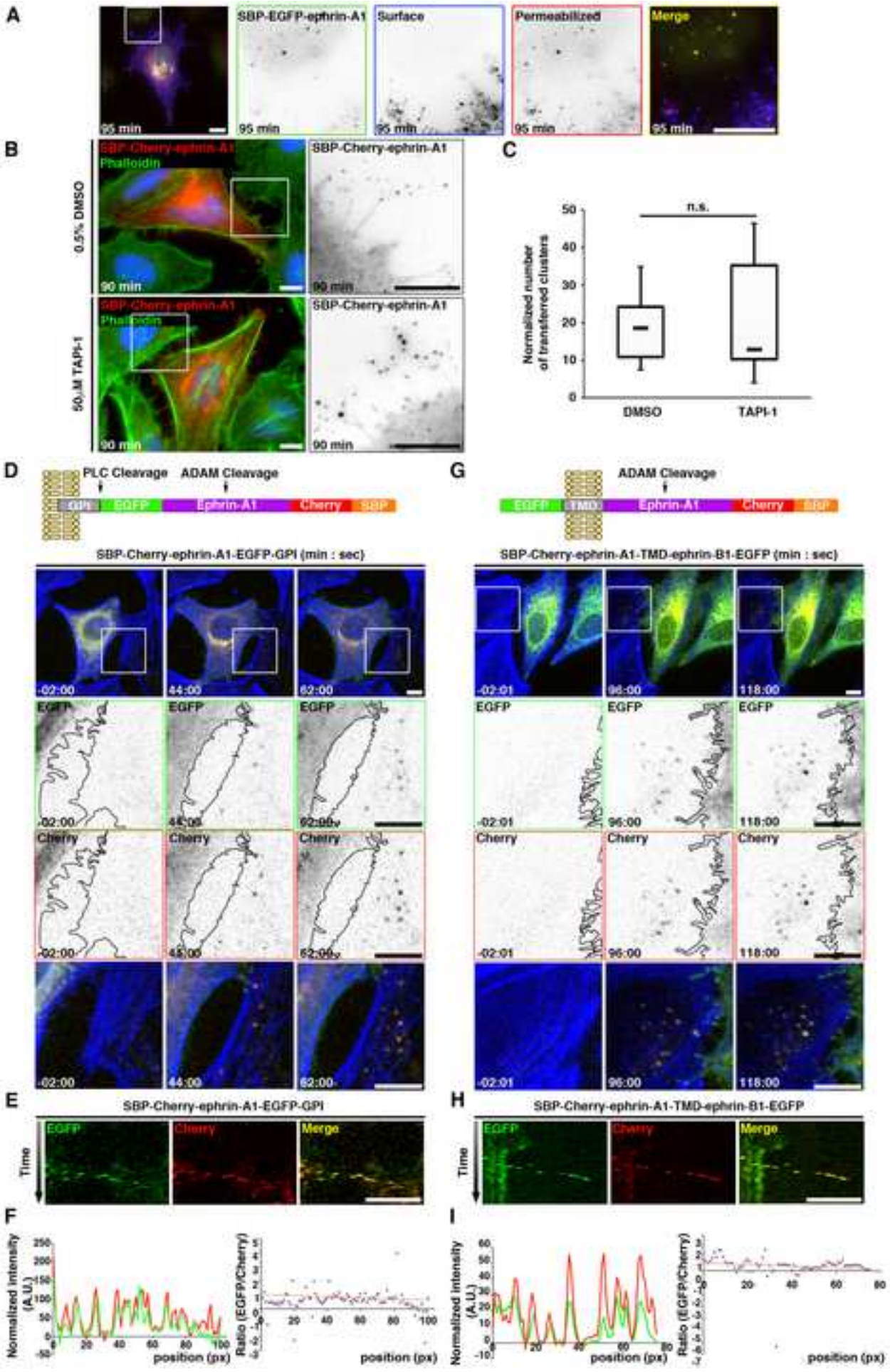

Figure 4

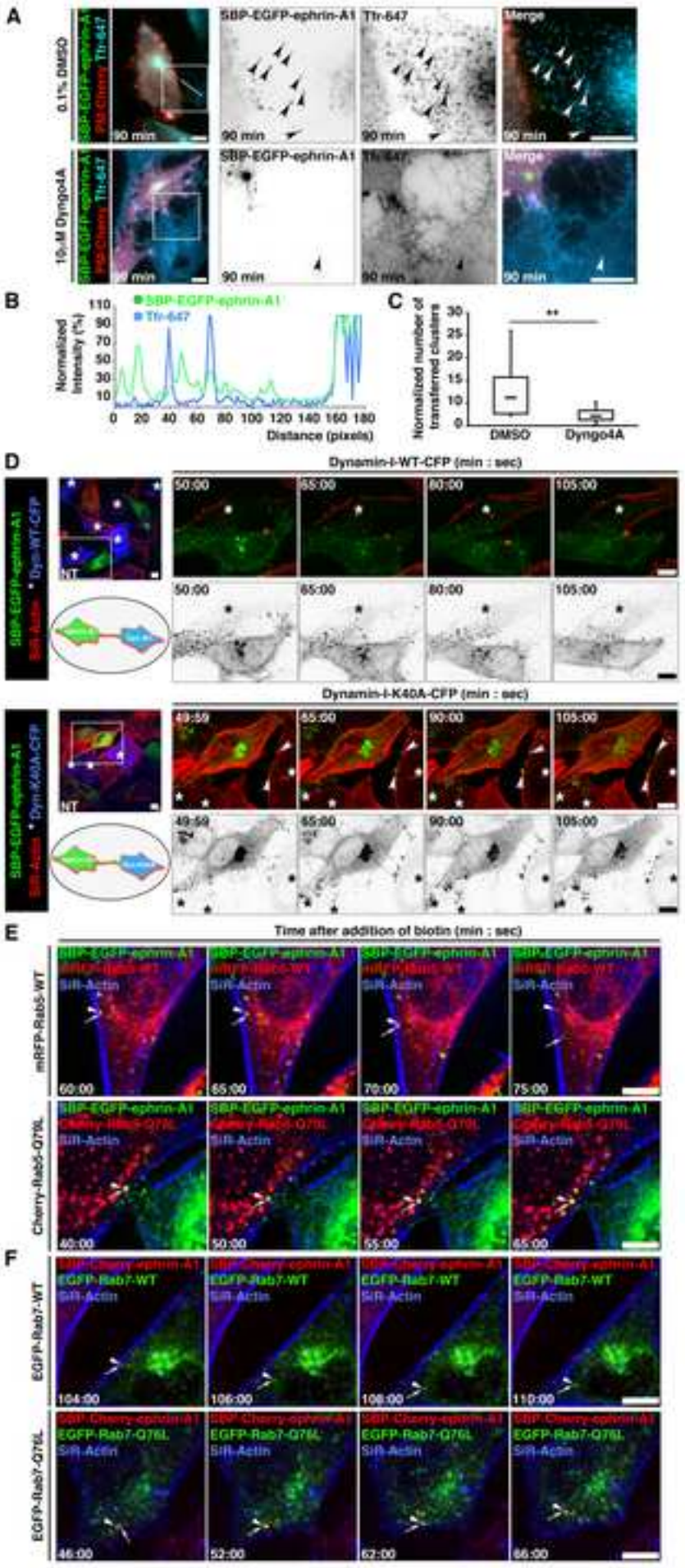

Figure 5

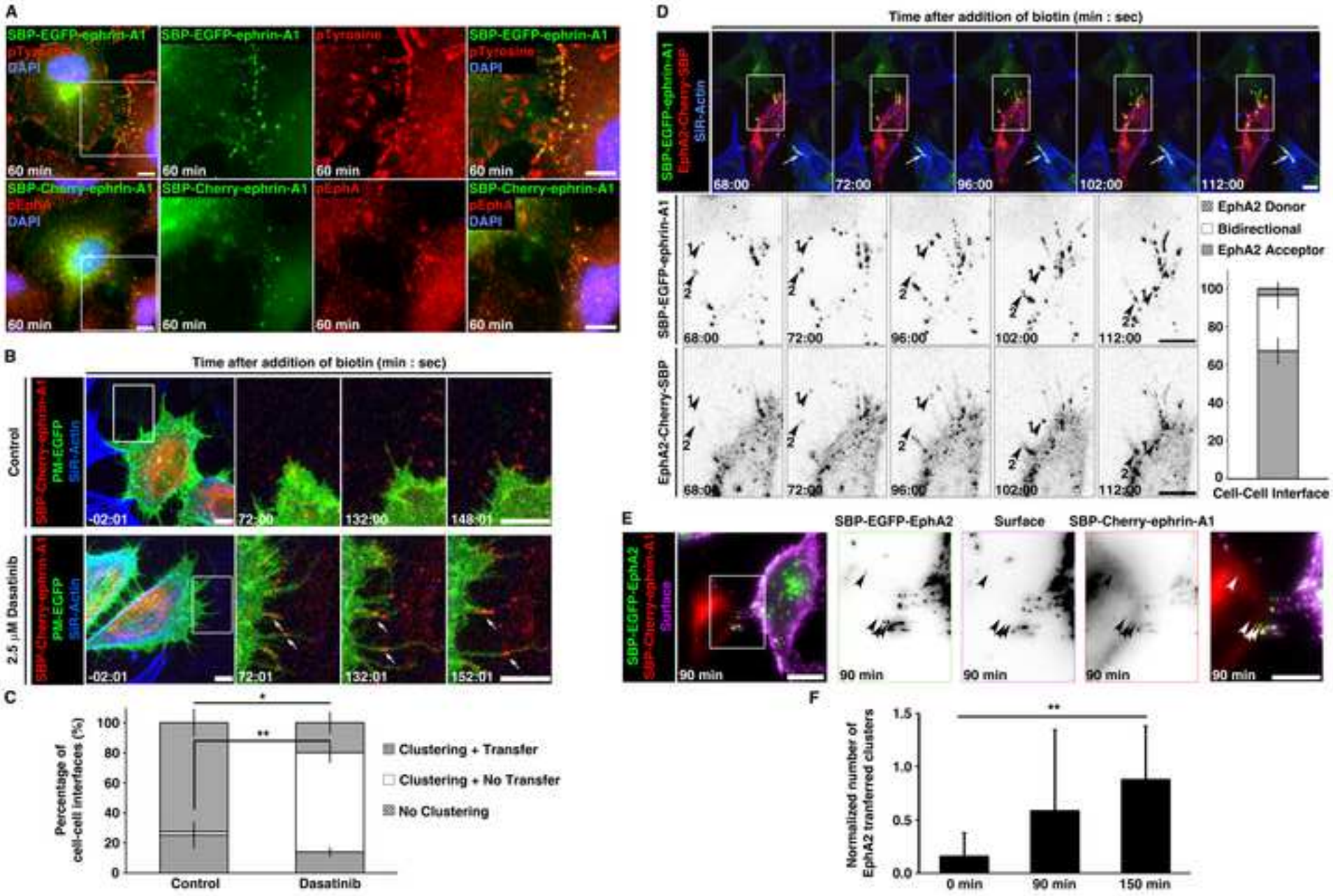

Figure 6

Click here to access/download;Figure;Figure6.tiff

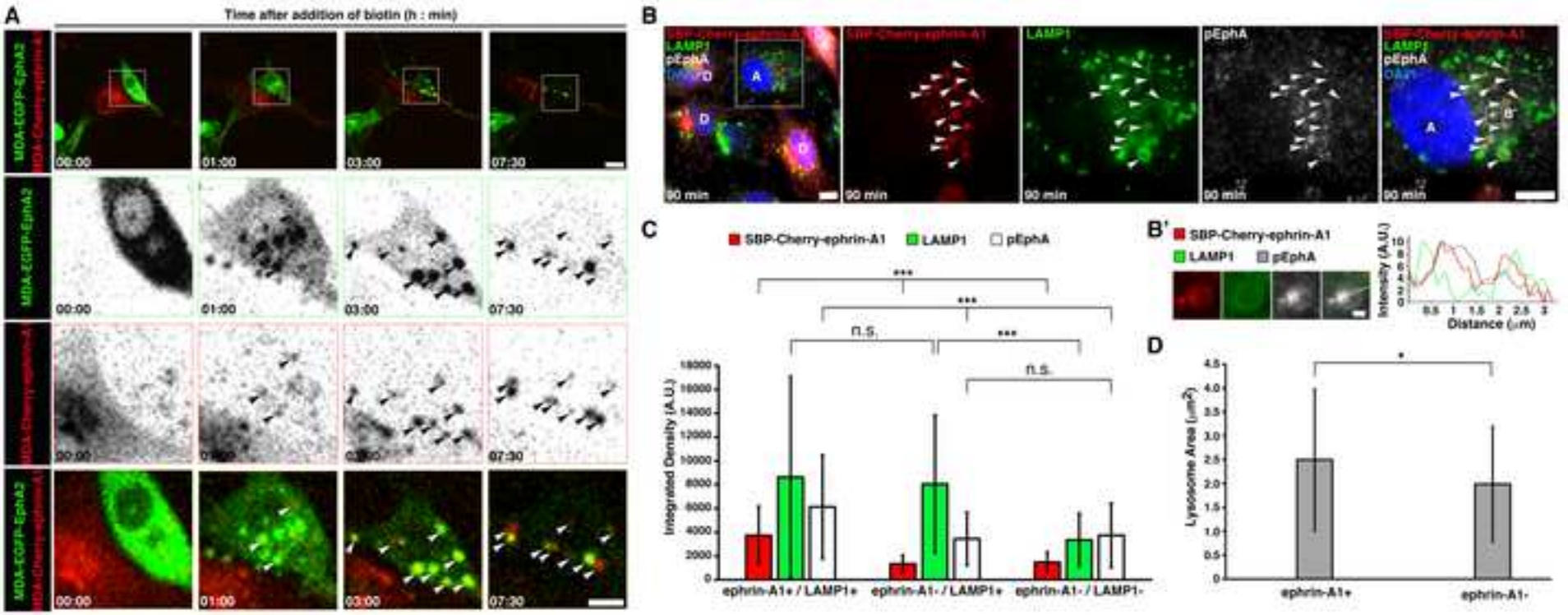

Figure 7

Click here to access/download;Figure;Figure7.tiff

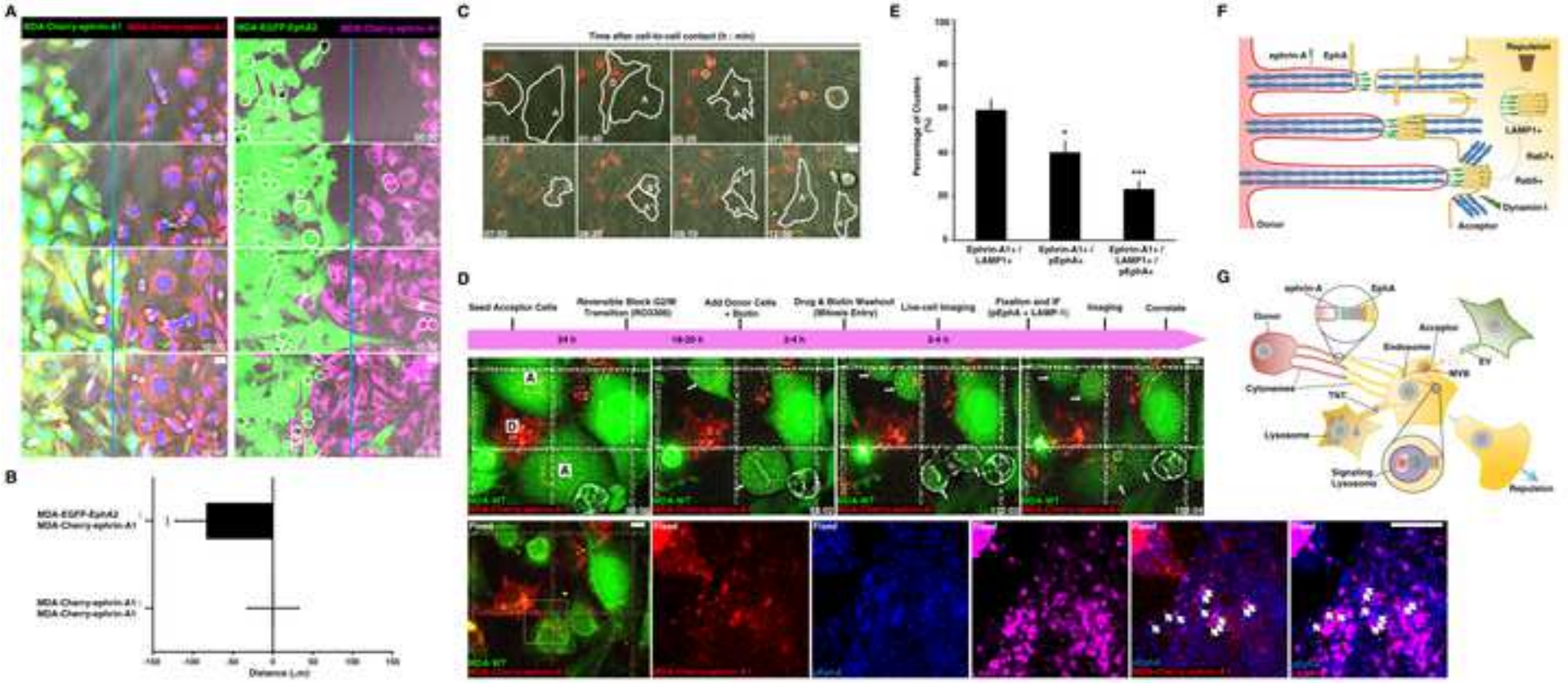

SUPPLEMENTARY FIGURES

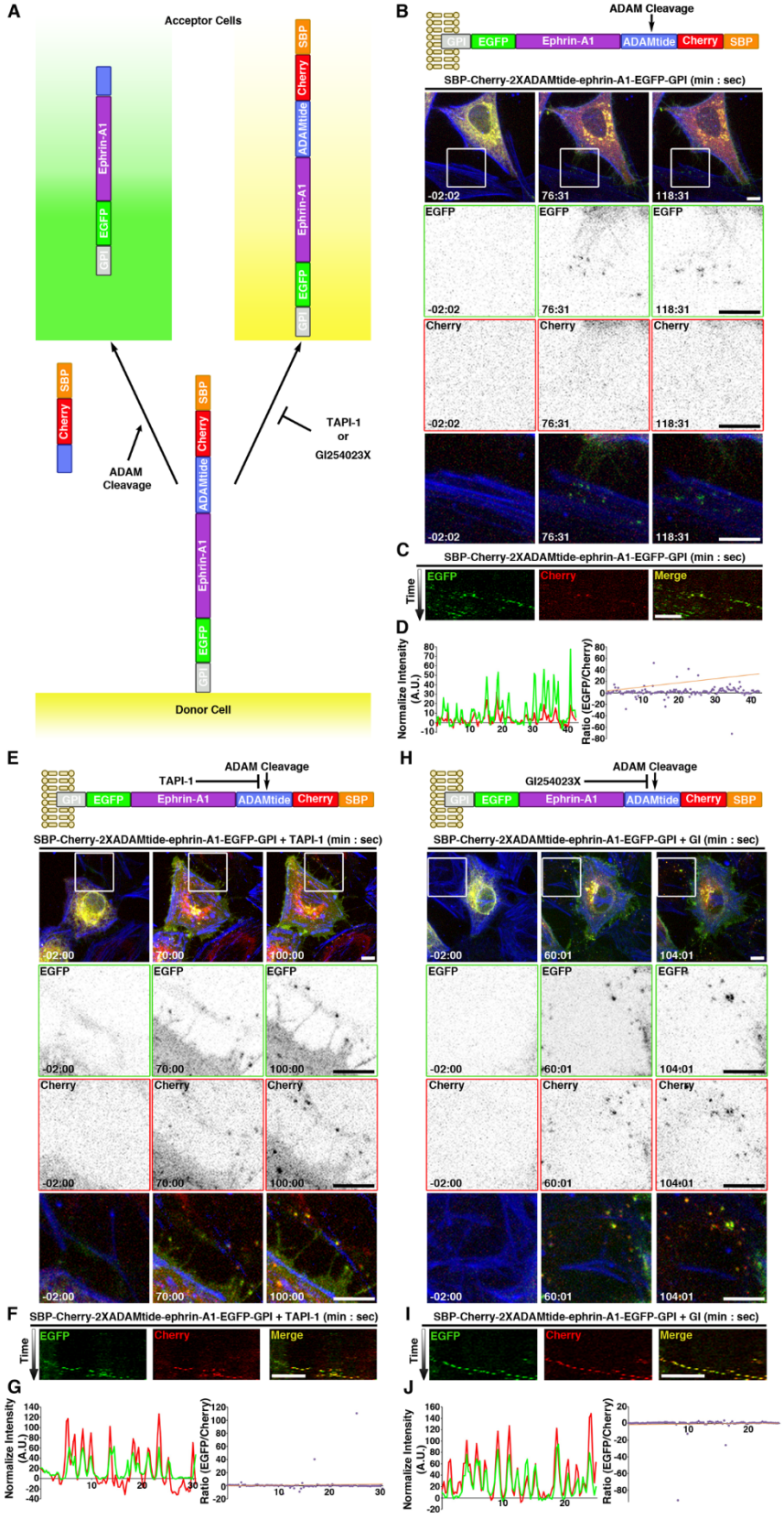

Supplementary Figure 1 Synthetic sensor of ADAM protease-based trans-endocytosis of ephrin-A1 (Related to Figure 3)

(A) Scheme of the experimental design of the ADAM-cleavage sensor SBP-Cherry-2XADAMtide-ephrin-A1-EGFP-GPI. The blue fragment represents the position of the inserted repetitions (2x) of the consensus ADAM cleavage site (ADAMtide).

(B) Time-lapse imaging of HeLa cells transfected with the SBP-Cherry-2XADAMtide-ephrin-A1-EGFP-GPI sensor. EGFP and Cherry signals are shown. Cell-cell boundaries are visualized with the actin probe SiR-Actin (blue). Bottom panels (high-magnification images of a donor/acceptor cell interface).

(C) Kymograph analysis of one cluster of SBP-Cherry-2XADAMtide-ephrin-A1-EGFP-GPI into an acceptor cell.

(D) Line-scan analysis and EGFP/Cherry intensity ratio obtained from the kymograph in (C).

(E-G) Same as in (B-D), but for cells treated with the metalloprotease's inhibitor TAPI-1.

(H-J) Same as in (B-D), but for cells treated with the ADAM-10 inhibitor GI254023X.

(B-C, E-F, H-I) Scale bars, 10 μm.

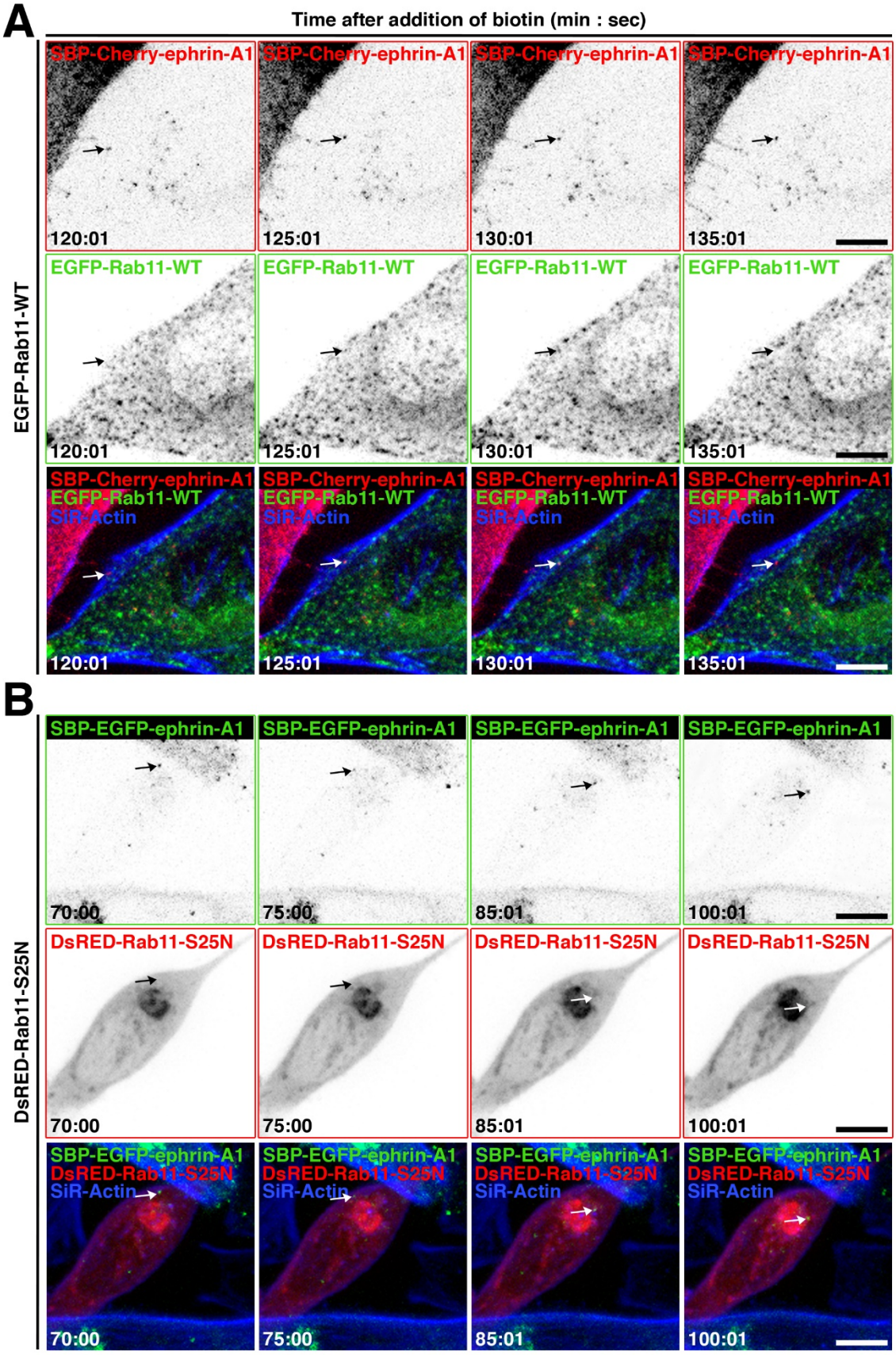
A
Time after addition of biotin (min : sec)
EGFP-Rab11-WT
SBP-Cherry-ephrin-A1
120:01
125:01
130:01
135:01
EGFP-Rab11-WT
SiR-Actin
B
DsRED-Rab11-S25N
SBP-EGFP-ephrin-A1
70:00
75:00
85:01
100:01

Supplementary Figure 2 Trans-endocytosed ephrin-A1 is sorted apart from Rab11-recycling endosomes (Related to Figure 4)

(A) Time-lapse imaging of HeLa cells expressing SBP-Cherry-ephrin-A1 co-cultured with cells expressing EGFP-Rab11-WT. Single channels are shown in inverted colors for better visualization (ephrin-A1 in the top row and Rab11 in the middle row). Merge images are shown (bottom panels: ephrin-A1, red; Rab11, green). Cell-cell interfaces were visualized by the SiR-Actin labeling (blue). Arrows indicate an example of trans-endocytosed SBP-Cherry-ephrin-A1 cluster in an acceptor cell.

(B) Same as in (A) but for cells expressing SBP-EGFP-ephrin-A1 (top row) and co-cultured with cells expressing DsRED-Rab11-S25N mutant (middle row).

(A-B) Scale bars, 10 μm.

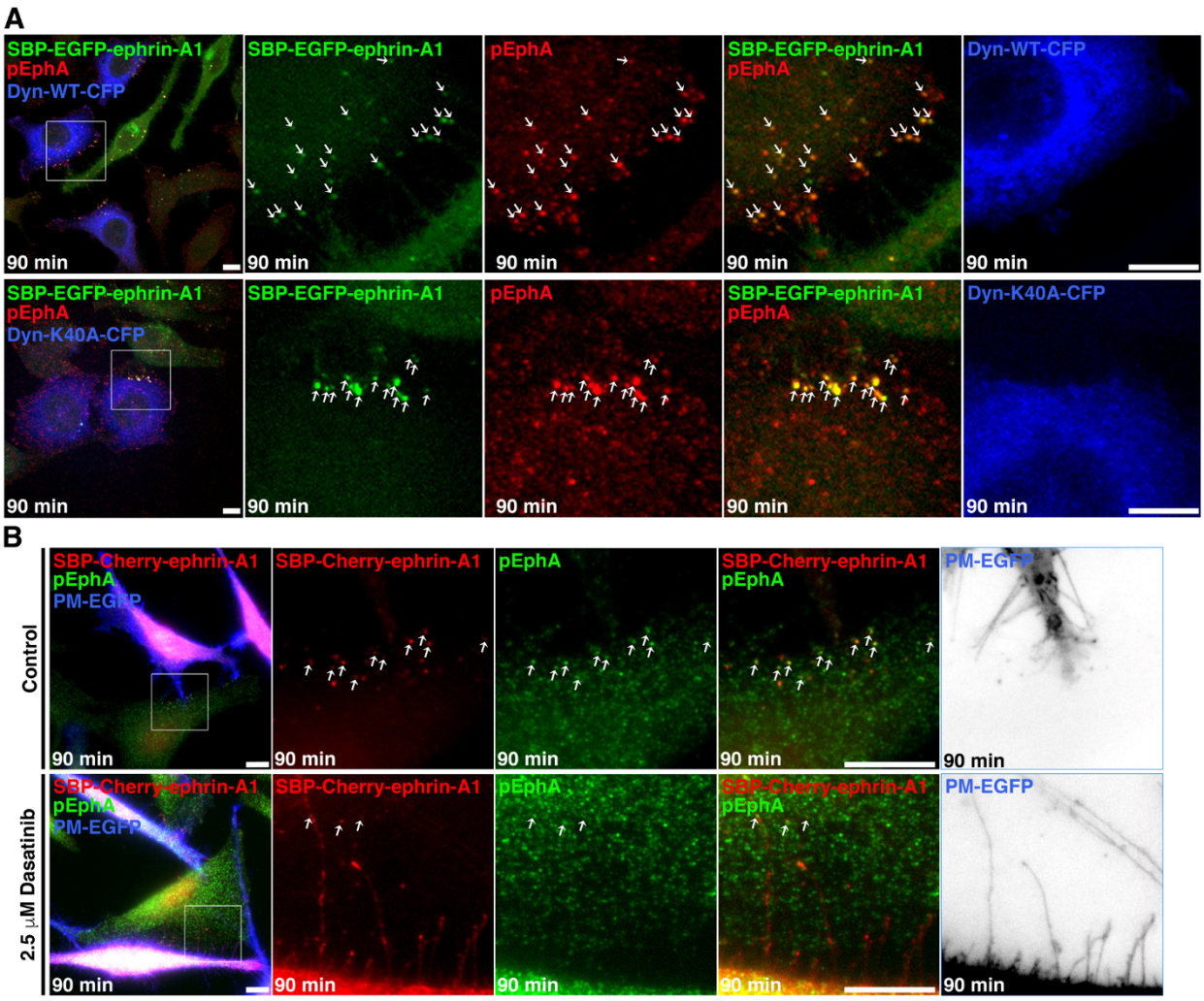

Supplementary Figure 3 Activation of EphA receptors at the plasma membrane is necessary for ephrin-A1 trans-endocytosis (Related to Figure 5)

(A) HeLa cells expressing SBP-EGFP-ephrin-A1 (green) were co-cultured with HeLa cells expressing Dynamin-I-WT-CFP (blue, top panels) or Dynamin-I-K44A-CFP (blue, bottom panels). Cells were treated with biotin (90 min), fixed and stained with an antibody against active phosphorylated EphA receptors (pEphA, red). Right panels show high-magnification images of the boxed area. Arrows indicate examples of trans-endocytosed SBP-EGFP-ephrin-A1 clusters in an acceptor cell co-localizing with active EphA receptors.

(B) HeLa cells co-expressing SBP-Cherry-ephrin-A1 (red) and PM-EGFP (blue), under control conditions (upper panels) or after EphA2 signaling inhibition with Dasatinib (bottom panels). Cells were fixed after 90 min of biotin addition. Immuno-staining with an antibody against active phosphorylated EphA receptors (pEphA, green) are shown. Right panels show high-magnification images of donor/acceptor cell interfaces (boxed area in the left panel). Arrows indicate examples of trans-endocytosed SBP-Cherry-ephrin-A1 clusters in an acceptor cell co-localizing with active EphA receptors. PM-EGFP is show in inverted colors (right panels) to highlight the long donor filopodia inside the acceptor cell after EphA receptor inhibition.

(A-B) Scale bars, 10 μm.

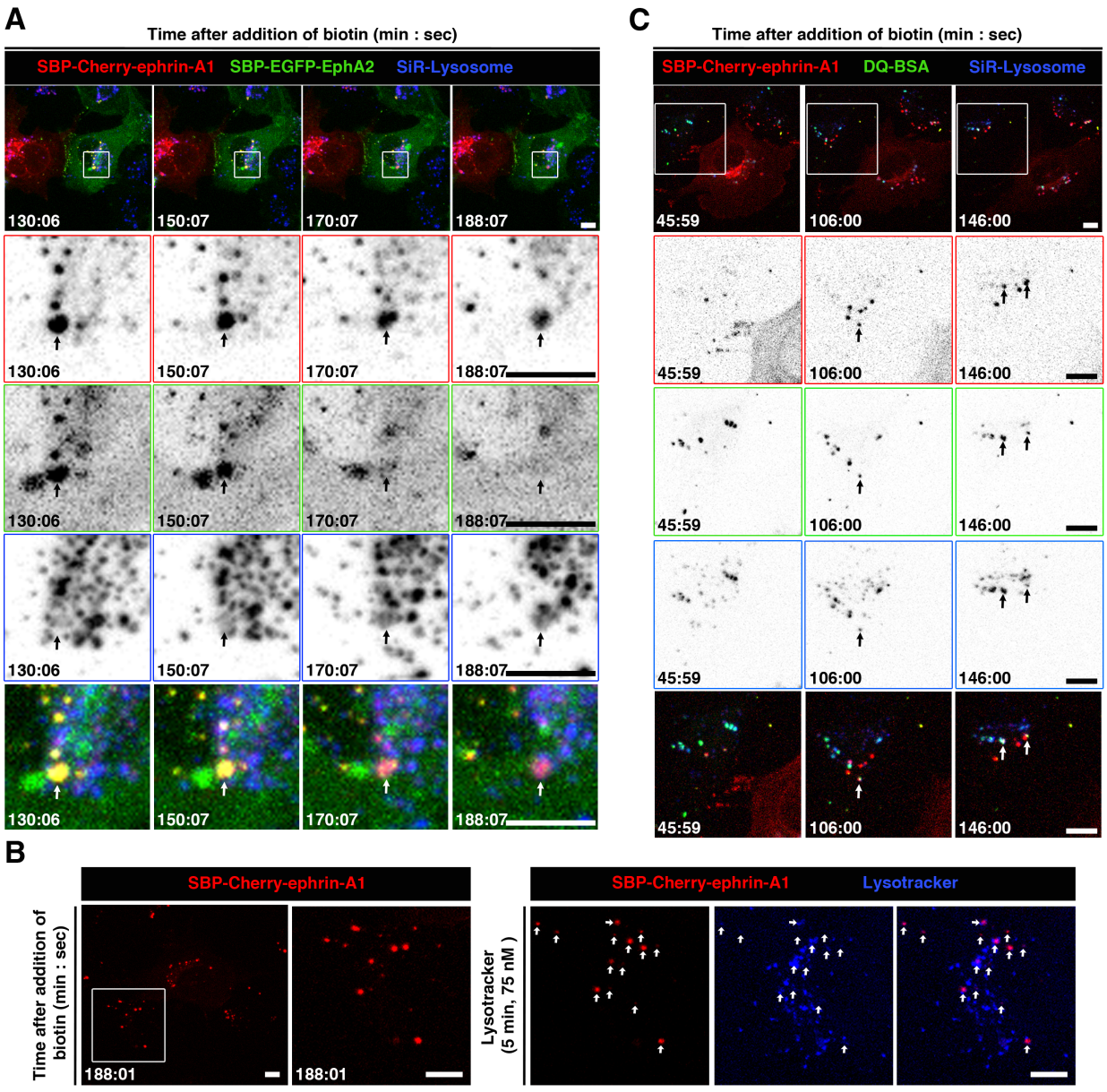

Supplementary Figure 4 Trans-endocytosed ephrin-A1 is co-transported with EphA2 and stored for a long time in acidic lysosomes in MDA-MB231 cells (Related to Figure 6)

(A) Live-cell imaging of MDA-MB231 cells stably expressing the RUSH construct SBP-Cherry-ephrin-A1 (SBP-Cherry-ephrin-A1, red) co-cultured with MDA-MB231 cells expressing steady-state SBP-EGFP-EphA2 (SBP-EGFP-EphA2 in the absence of hook

expression, green). Lysosomes were stained with the SiR-lysosome dye (blue). High-magnification images are presented below in black and white: SBP-Cherry-ephrin-A1 (top row), SBP-EGFP-EphA2 (middle-upper row) and SiR-lysosome (middle-lower row). Merge images are shown (bottom row). Arrows indicate an example of a trans-endocytosed SBP-Cherry-ephrin-A1 cluster co-transported with SBP-EGFP-EphA2 towards a large lysosomal structure in an acceptor cell.

(B) Single frame from live-cell imaging of MDA-MB231 cells stably expressing the RUSH construct SBP-Cherry-ephrin-A1 (SBP-Cherry-ephrin-A1, red) co-cultured with wild-type MDA-MB231 cells (left pannel). High magnification images of an acceptor cell are shown. Right panels shown the same cell after a short treatment with the acidotrophic dye Lysotracker (blue). Arrows indicate trans-endocytosed SBP-Cherry-ephrin-A1 in acidic lysosomes.

(C) Live-cell imaging of MDA-MB231 cells stably expressing the RUSH construct SBP-Cherry-ephrin-A1 (SBP-Cherry-ephrin-A1, red) co-cultured with wild-type MDA-MB231 cells. Lysosomes were stained with the SiR-lysosome dye (blue). Degradative compartements were detected by the fluorogenic protease substrate DQ-BSA (green). High-magnification images are presented below in black and white: SBP-Cherry-ephrin-A1 (top row), DQ-BSA (middle-upper row) and SiR-lysosome (middle-lower row). Merge images are shown (bottom row). Arrows indicate trans-endocytosed SBP-Cherry-ephrin-A1 in degradative lysosomes.

(A-C) Scale bars, 10 μm.

Supplemental Video 1

Click here to access/download

Supplemental Videos and Spreadsheets

Video S1.mp4

Supplemental Video 2

Click here to access/download

Supplemental Videos and Spreadsheets

Video S2.mp4

Supplemental Video 6

Click here to access/download

Supplemental Videos and Spreadsheets

Video S6.mp4

Supplemental Video 9

Click here to access/download

Supplemental Videos and Spreadsheets

Video S9.mp4

Supplemental Video 3

Click here to access/download

Supplemental Videos and Spreadsheets

Video S3.mp4

Supplemental Video 4

Click here to access/download

Supplemental Videos and Spreadsheets

Video S4.mp4

Supplemental Video 5

Click here to access/download

Supplemental Videos and Spreadsheets

Video S5.mp4

Supplemental Video 7

Click here to access/download

Supplemental Videos and Spreadsheets

Video S7.mp4

Supplemental Video 8

Click here to access/download

Supplemental Videos and Spreadsheets

Video S8.mp4

Click here to access/download

Supplemental Videos and Spreadsheets

Video S10.mp4

Inventory of Supplemental Information

- **Valenzuela & Perez_Supplementary Materials** document
  - Supplementary Figure 1: Synthetic sensor of ADAM protease-based trans-endocytosis of ephrin-A1 (Related to Figure 3)
  - Supplementary Figure 2: Trans-endocytosed ephrin-A1 is sorted apart from Rab11-recycling endosomes (Related to Figure 4)
  - Supplementary Figure 3: Activation of EphA receptors at the plasma membrane is necessary for ephrin-A1 trans-endocytosis (Related to Figure 5)
  - Supplementary Figure 4: Trans-endocytosed ephrin-A1 is co-transported with EphA2 and stored for a long time in acidic lysosomes in MDA-MB231 cells (Related to Figure 6)

- **Supplementary movies**
  - Supplementary Video 1 (Related to Figure 1) Partial sorting of EphA2 and ephrin-A1 at the Golgi apparatus
  - Supplementary Video 2 (Related to Figure 1) Ephrin-A1 is exported from filopodia of ligand-producing cells
  - Supplementary Video 3 (Related to Figure 2) Ephrin-A5 is transferred to neighboring cells from filopodia
  - Supplementary Video 5 (Related to Figure 2) Actin-dependent trans-endocytosis of ephrin-A1 from filopodia
  - Supplementary Video 6 (Related to Figure 3) Cleavage-independent trans-endocytosis of ephrin-A1
  - Supplementary Video 7 (Related to Figure 4) Dynamin-dependent trans-endocytosis of ephrin A1
  - Supplementary Video 8 (Related to Figure 5) Localized trans-endocytosis of ephrin-A1/EphA2 complexes
  - Supplementary Video 9 (Related to Figure 5) Trans-endocytosis of ephrin-A1 is massive at steady state
  - Supplementary Video 10 (Related to Figure 7) Inheritance of trans-endocytosed ephrin-A1 in cancer cells